Silicon Fundamentals for Photonics Applications

David J. Lockwood[1] and Lorenzo Pavesi[2]

[1] Institute for Microstructural Sciences, National Research Council of Canada
Ottawa, ON, Canada K1A 0R6
David.Lockwood@nrc-cnrc.gc.ca
[2] Dipartimento di Fisica, Università di Trento
Via Sommarive 14, 38050-Povo Trento, Italy
pavesi@science.unitn.it

Abstract. The many and diverse approaches to materials science problems have greatly enhanced our ability to engineer the physical properties of semiconductors. Silicon, of all semiconductors, underpins nearly all microelectronics today and will continue to do so for some time to come. However, in optoelectronics and photonics, the severe disadvantage of an indirect band-gap and of a negligible electro-optic coefficient has limited the application of elemental silicon. This chapter provides introductory material on the physical properties of silicon and outlines a number of diverse approaches to engineering efficient photonic components from silicon. The common paradigm is material compatibility with microelectronic components.

1 Introduction

The ubiquitous silicon microelectronic "chip" is taken for granted in modern society. There has been much research involved in producing these high technology marvels and such research continues unabated at a faster and faster pace. Continued developments in Si and, more recently, $Si_{1-x}Ge_x$ alloy and strained silicon technology [1, 2] continue to advance the frontiers of device integration, complexity, and speed. This continued advance has been driven by application requirements in switching technology (e.g., computers) and high-speed electronics (e.g., wireless telecommunications). Today the thrust is towards pervasive computing: the end-user will use all the power of a computer without noticing that the device he is using has a computer inside. Other compound semiconductor materials, such as GaAs or InP or III–V alloys, have, however, maintained a significant role in the construction of optoelectronic and purely photonic devices [3]. Photonics is the technology associated with signal generation, processing, transmission and detection where the signal is carried by photons (i.e., light); principal photonic devices are lasers, waveguides, modulators, detectors, and optical fibers [4].

If one compares today's photonics industry (worth almost 9 b$) with the microelectronics one (worth almost 160 b$) there are many differences:

L. Pavesi, D. J. Lockwood (Eds.): Silicon Photonics, Topics Appl. Phys. **94**, 1–52 (2004)

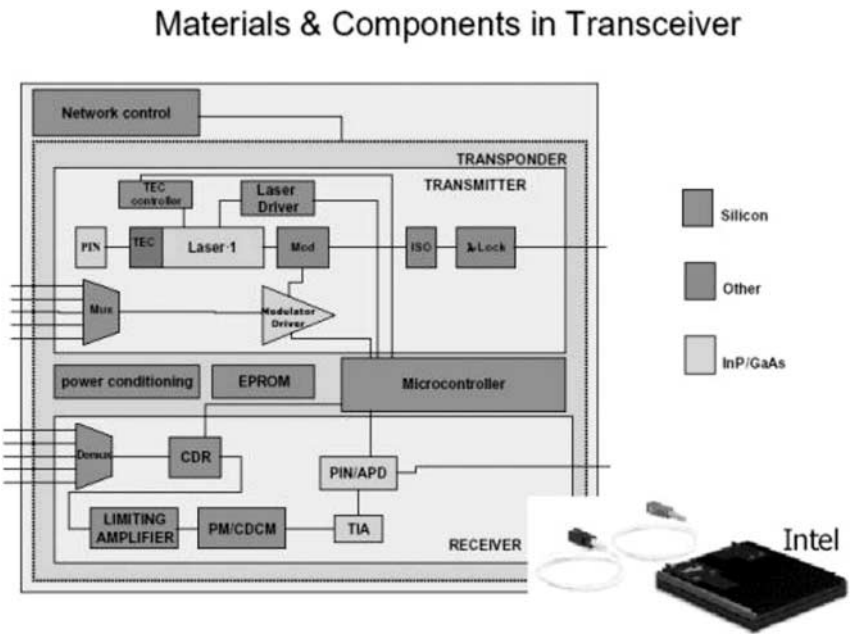

Fig. 1. Materials and components in an optoelectronic transceiver. (Source: Intel ©)

- A variety of different materials is used: e.g., the InP substrate for source development, silica as the material for fibers, lithium niobate for modulators, other materials for DWDM components and EDFA amplifiers, and so on (see Fig. 1).
- No single material or single technology is leading the market. Some convergence is appearing towards the use of InP as the substrate material to integrate different optical functions. However, other materials are potential candidates for overcoming the limitations of InP.
- The industry is characterized by many different small companies that are specialized in producing specific devices: e.g., lasers, modulators, etc. No large companies are dominating this field at present.
- The production technology is still very primitive. Chip scale integration of optical components, which enables low cost and high reproducibility, has not yet been achieved. Neither the standardization of processes nor of the packaging of optical components, which is inherent for mass production and repeatability, are present.
- Roadmaps to dictate and forecast the evolution of photonics are only now being elaborated. It is commonly accepted that the industrial model of microelectronics, if applied to photonics, will give a substantial boost to the development and implementation of photonics. All the big manufactur-

ers of microelectronics have aggressive programs to develop microphotonic devices, mostly based on silicon.

The merging of Si-based electronics with photonics has largely required the pursuit of hybrid technologies for light emitters and modulators (see, for example, [5]), which are often both expensive and complicated to produce. Given that Si light emitters and, in particular, lasers, are not yet commercially available for on-chip optoelectronic applications, considerable effort is being placed on marrying dissimilar materials to fashion hybrid devices utilizing Si microelectronics [5, 6]. For example, monolithically integrated GaAs efficient light emitting diode (LED) arrays with Si driver circuits have been created [7], and integrated photonic circuits where active III-V lasers and diodes are merged with passive silicon based optical components are commercially available [8]. However, the main interest is in combining III–V semiconductor laser diodes with Si integrated circuits for optical fiber communications or optical interconnects. The main issue to be faced is the potential enormous market of fiber-to-home applications. This requires the growth of III–V materials such as GaAs or InP on Si followed by processing, or the direct bonding of III–V laser devices detached from their substrates via an epitaxial lift-off process [9, 10]. Both methods have their disadvantages.

The lattice mismatch of 4% between GaAs and Si, the different thermal expansion coefficients and the fact that Si is a fast diffusing impurity for III–V semiconductors create severe difficulties in maintaining the required low defect density in GaAs for laser production. dislocations produced by relaxation of the GaAs epitaxial layer are detrimental to device performance and life. Various methods are being tried to alleviate this problem [11] including Ge, superlattice, or graded buffer layers between Si and GaAs, but other difficulties arise from the high GaAs growth temperatures. Despite all these difficulties, a few industrial companies have claimed recently the invention of heteroepitaxial procedures that could potentially boost the development of hybrid optoelectronic integration. Nitronex has pioneered a proprietary technology called “Pendeoepitaxy” that grows GaN crystals over SiC substrates or over Si substrates after the growth of a SiC buffer layer. A reduction in defect density of many orders of magnitude relative to other growth techniques can be obtained. This technology enables the integration of high quality GaN with Si [12]. *Motorola Labs* have developed a technique based on a Strontium titanate (STO) buffer layer. By growing thick STO layers, oxygen atoms diffuse through STO and locate at the STO/Si interface, forming an amorphous interface between crystalline Si and crystalline STO. The STO layer relaxes and allows the successive epitaxial growth of GaAs layers [13]. These new techniques have just been developed and thus it is impossible to tell yet how Si optoelectronics will be affected by them.

The epitaxial lift-off technique is more straightforward, involving wet chemical etching of a release layer, floating off the III–V heterostructure, and transferring it to a planar Si substrate, where it bonds via the van der

Waals force [9,10]. It is essential for this bonding technique to work that the substrate surface be chemically clean and free of particles.

Wafer fusion involves bringing the two materials of high quality into intimate contact under hydrogen ambient at temperatures of around 450 °C. Subject to a uniform directly-applied pressure, the substrates form robust chemical bonds over times of the order of 30 min. Selective chemical etching allows for the removal of one of the substrates, resulting in a thin film of one material bonded to a substrate of another, and the interface between them is quite free of threading dislocations. Wafer fusion has been demonstrated in many materials systems, although from the point of view of devices the technique is still in its infancy. The usual approach comprises bonding composite semiconductor films onto thicker Si substrates. For example, optoelectronic elements such as InGaAs/GaAs strained quantum well lasers [14] and InP lasers [15] have been bonded to Si. GaP/Si wafer-bonded heterojunctions have recently been demonstrated and suggested for optoelectronics [16].

A different approach has been suggested by *Fonstad* et al. [17]. They point out that optoelectronic devices are intrinsically very thick devices (typically at least a micrometer thick), and thus, if they are bonded on a Si substrate in the usual approach, they are very sensitive to stress. On the other hand, Si MOS transistors need only be a few tens of nanometers thick and are much less stress sensitive. Therefore, they suggest retaining a GaAs substrate so that the intrinsically thick, inherently strain- and defect-sensitive optoelectronic devices see their optimum substrate (i.e., GaAs). The SOI technique would be a possibility to produce Si CMOS electronics on GaAs substrates without sacrificing any of the performance of the CMOS. They term this technology silicon-on-gallium arsenide (SonG). The SonG process combines Si and GaAs substrates by wafer bonding.

Other problems are associated with the change in crystal structure from non-polar Si to polar GaAs. A non-planar Si growth surface can lead to stacking faults in the GaAs and there is charge build-up at the Si-GaAs interface [10]. The 8% lattice mismatch for InP on Si is even worse than for GaAs leading to even more severe heteroepitaxy growth problems. Even so, by use of a thick GaAs buffer layer, a 1.54 μm wavelength InGaAs/InGaAsP multiple quantum well laser operating continuously at room temperature has been produced on a Si substrate [18]. Recently InAs quantum dot lasers have been directly grown on Si [19]. In addition the use of Si as a substrate for III–N blue lasers is becoming more and more important [20]. Further significant progress in many of these areas can be anticipated within the next few years, and commercial devices will follow once the scaling up of these techniques to the mass production level has been achieved.

The most satisfactory solution would be optoelectronic and photonic devices created entirely from Si-based materials, where the extensive experience in Si fabrication and processing could be put to best use. The major deficiency in Si-based optoelectronic devices remains the lack of suitable light

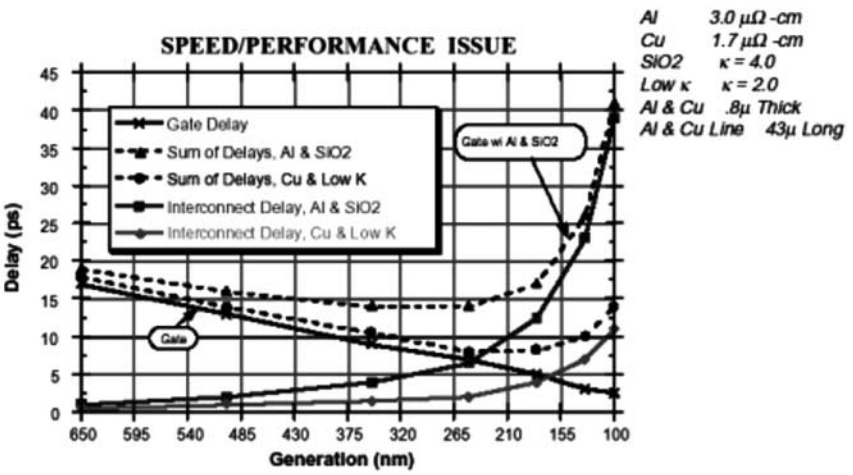

Fig. 2. Calculated gate delay and wire delay as a function of the minimum feature size (device generation). From SIA Roadmap 1997 [27]

emitters and especially lasers. Research in this field is rapidly progressing and amongst the most recent results are the observation of net optical gain in silicon nanocrystals [21], and the demonstration of an LED with a power efficiency in excess of 1% in porous silicon (PS) [22] or more than 20% in Er-doped silicon rich oxide. Some companies are claiming the availability of high-efficiency infrared Si diodes [23], the first release of a commercial device based on an all-silicon opto-coupler [24], and the measurement of net optical gain in semiconductor grade silicon [25].

The general requirements in Si-based light sources are LEDs, lasers, and optical amplifiers for use in electronic devices, optical devices and displays. Operating wavelengths in the range 0.4 μm–1.6 μm are needed to cover both full-color displays and the transparency windows of optical fibers at the operating wavelengths of 1.3 μm and 1.55 μm. Specific applications for such sources include fiber-optic transmitters, optical interconnects within and between computer chips and boards, optical controllers for phased-array microwave antennas, information display screens, printing elements in xerography, and writing and readout of optical compact disc information.

Especially important are applications of optical interconnects related to the limitations of the operating speed of microelectronic devices created by the interconnect bottleneck [26]. Figure 2 shows the signal delay as a function of the transistor generation [27]. For a gate length shorter than 200 nm, a situation is reached where the delay is no longer dictated by the gate switching time but by the wiring delay. In addition, the length of interconnects on a single chip are getting longer and longer. Nowadays chips have a total interconnection length per unit area of the chip of some 5 km/cm^2 with a chip area of 450 mm^2 while in ten years from now these lengths will become

20 km/cm^2 for a chip area of 800 mm^2. The problem is not only related to the length of interconnect but also to the complexity of their architecture. Nowadays, there are 6 levels of metal layers, while in ten years from now they will become greater than 12. All these facts introduce problems related to the delay in signal propagation caused by resistance-capacitive coupling, signal latency, signal cross-talk, and resistance-inductive delays due to the reduction in dimensions and increase in density of the metal lines. Finally, there is the problem of power consumption and heat dissipation, which causes the thermal power generated within the chip to reach a density in excess of a conventional hot-plate and within few years to reach the level typical of nuclear reactors. A possible solution to these problems is looked for in optical interconnects [28]. Nowadays optical interconnects utilizing optical fibers and III–V laser sources are already used to connect different computers or peripherals. It is predicted that optical interconnects will be used to connect computer boards in five years, while optical interconnects within the chip will be used in ten to fifteen years from now [29]. The need for optical interconnects is one of the main motivations to develop silicon photonics.

To alleviate the miserable light emission in bulk Si ($\sim 10^{-6}$ quantum efficiency at 300 K in standard electronic grade silicon, where the quantum efficiency is defined as the ratio of the number of photons generated over the number of excited electron–hole pairs), many quite different approaches have been proposed and are actively being explored [30]. Some, such as $Si_{1-x}Ge_x$ quantum well or Si/Ge superlattice structures, rely on band structure engineering, while others rely on quantum confinement effects in low dimensional structures, as typified by quantum dots or PS. Still another approach is impurity-mediated luminescence from, for example, isoelectronic substitution or by the addition of rare earth ions. A brief overview of results obtained with these and other methods is given below. However, in order to understand more fully the reasons why such different approaches are necessary, it is appropriate to review first what creates the optical emission problem in crystalline Si (c-Si).

2 Physical Properties of Silicon

Silicon crystallizes in the diamond structure [31], which consists of two interpenetrating face-centered cubic lattices displaced from each other by one quarter of the body diagonal. In zinc-blende semiconductors such as GaAs, the Ga and As atoms lie on separate sublattices, and thus the inversion symmetry of Si is lost in polar III–V binary compounds. The difference in the crystal structures underlies the disparate electronic and optical properties of Si and GaAs and results in the slow optical response of Si together with its small electro-optic coefficient. The energy band structure in semiconductors is derived from the relationship between the energy and momentum of a charge carrier, which depends not only on the crystal structure but also on

the bonding between atoms, the respective bond lengths, and the chemical species. The band structure is often quite complex and can only be calculated empirically. The results of such calculations [32] for Si and GaAs are shown in Fig. 3. The figure shows the dispersion relations for the energy $E(\boldsymbol{k})$ of an electron (positive energy) or hole (negative energy) for wave vectors $\boldsymbol{k}$ within the first Brillouin zone.

The valence band structure is generally similar for many semiconductors and exhibits a maximum at the Brillouin zone center or Γ point (i.e., at $\boldsymbol{k} = 0$). The notable difference between Si and GaAs is that the degeneracy in the $\Gamma_{25'}$ band maximum at $\boldsymbol{k} = 0$ is removed in the case of GaAs, because of the spin-orbit interaction, into Γ_7 and Γ_8 sub-bands. In general, $E(\boldsymbol{k})$ has maxima or minima at zone center and zone boundary symmetry points, but additional extrema may occur at other points in the Brillouin zone (see Fig. 3). In the case of Si, the lowest point in the conduction band occurs away from high symmetry points near the X point at the Brillouin zone boundary (along $\langle 001 \rangle$), whereas in GaAs it occurs at the Γ point. The energy gap in a semiconductor is defined as the separation between this absolute conduction band minimum and the valence band maximum at the Γ point. For GaAs, the energy gap is classified as direct, because the maximum and minimum occur at the same $\boldsymbol{k}$ and an electronic transition can occur directly at $\boldsymbol{k} = 0$ between initial and final states having the same wave vector. Correspondingly, Si is termed an indirect gap semiconductor, because the initial and final states have different wave vectors.

Optical transitions conserve both energy and momentum. In direct gap GaAs, an excited electron at the bottom of the conduction band can relax spontaneously back into a hole in the valence band by emitting a photon at the band-gap energy with momentum conservation (the photon momentum is negligible with respect to the electronic one). This electron–hole radiative recombination process can only occur in Si with the assistance of a further process to conserve the momentum. This, in pure Si, occurs via the transfer of the electron momentum to a phonon that is created with equal and opposite wave vector to that of the initial state in the conduction band. Such a three-body process is quite inefficient compared with direct gap recombination [33, 34]. Thus, the probability of spontaneous emission is very low for Si and high for GaAs. Alternatively, by relating the recombination probability to a characteristic recombination lifetime, the spontaneous emission or radiative lifetime in silicon is very long (millisecond range) while in direct gap III–V semiconductors it is short (nanosecond range). In general, when excited carriers relax, non-radiative recombination pathways compete with radiative recombination. This competition is strongly thrown off balance for normal Si, because of the long radiative lifetime, and hence non-radiative recombinations are dominant which in turn cause the very low luminescence efficiency. However, when high purity and surface passivated silicon is used,

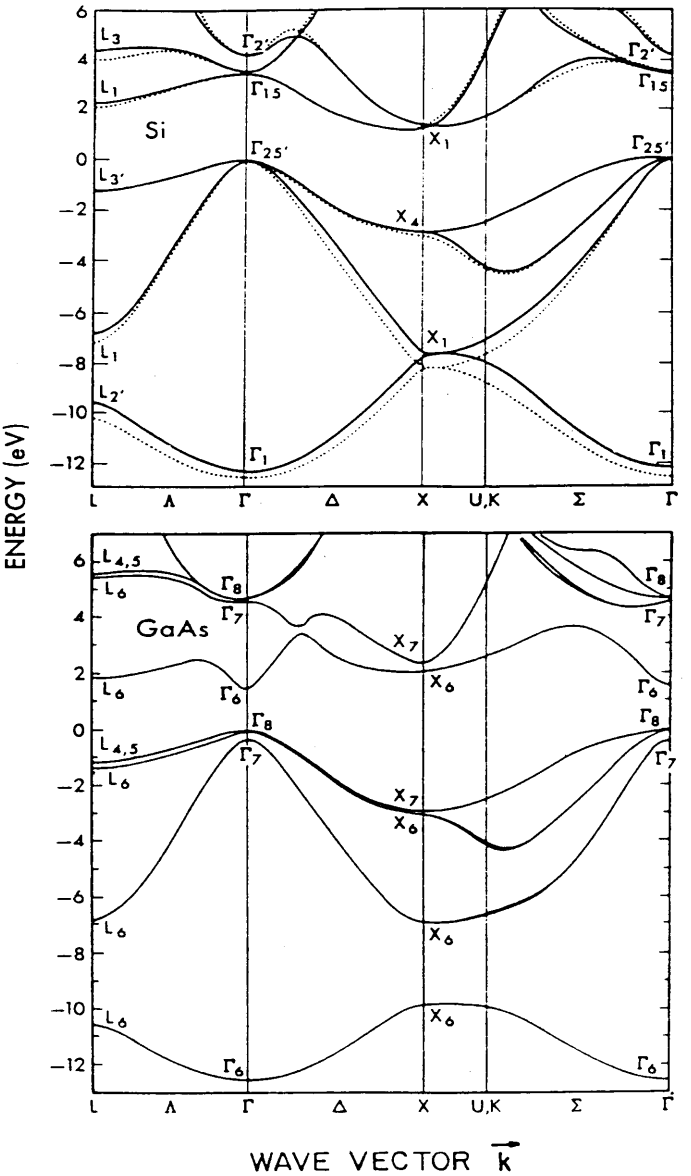

Fig. 3. Theoretical band structures of Si and GaAs. In the case of Si, results are shown for nonlocal (*solid line*) and local (*dashed line*) pseudopotential calculations. After [32]

high luminescence efficiency can be achieved although still with a very long recombination time [35].

The indirect band-gap of Si is 1.12 eV at room temperature (see Fig. 3). The weak band-to-band emission at this energy in the near infrared was first observed by *Haynes* and *Briggs* [36] using visible light excitation or by forward-biasing Si diodes. A review of the work on intrinsic and extrinsic radiative recombination in Si has been given by *Dean* [37] and more recently by *Davies* [38].

Electron–hole pairs created either optically or electrically in Si may bind to each other to form excitons, which can be either free or tied to impurities or defects [33,34]. Exciton recombination dominates the optical emission process at low temperatures and is characterized by very narrow emission lines. At high temperatures, however, excitons are thermally dissociated and emission is due to direct band-to-band recombination. Excitonic emission is under active investigation in quantum well, wire, and dot structures corresponding to carrier confinement in one, two and three dimensions, respectively [39].

Materials engineering, a relatively new phenomenon in materials science, is now being actively applied to Si in an attempt to overcome the indirect band-gap limitations in light emission from Si. In these various attempts, the aims are:

- to increase the efficiency of the luminescence by increasing the overlap of the electron and hole wavefunctions via, for example, quantum confinement and band structure engineering or by spatially confining the exciton in a defect-free region so that nonradiative recombination lifetimes become very long,
- to tune the wavelength of the emission by forming alloys, molecules, and clusters,
- to induce recombination at impurity centers, or
- to use intraband transitions (e.g., within the valence band) where the indirect band-gap of Si does not play any further role.

Such attempts can often involve several of these factors. Each of these methods is outlined below.

3 Band-Gap Engineering

3.1 Brillouin Zone Folding in Atomic Layer Superlattices

Some 25 years ago *Gnutzmann* and *Clausecker* [40] conjectured that Brillouin zone folding in thin layer superlattices where the layer thicknesses were of the order of the unit cell dimensions could result in a direct (or quasi-direct, as it is now termed) band-gap structure. The growth in the 1980s of high quality $(\mathrm{Si}_m\mathrm{Ge}_n)_p$ atomic layer superlattices (m and n are the number of monolayers of Si and Ge in each period and p is the number of periods) by molecular

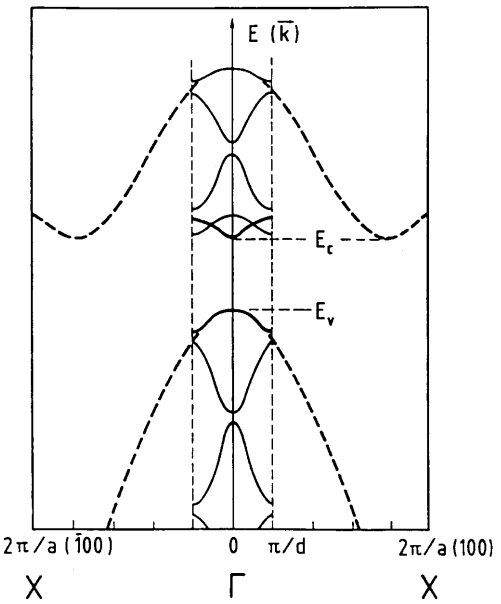

Fig. 4. Schematic representation of the Brillouin zone folding concept in Si resulting from the new superlattice periodicity in the growth direction. Here, the conduction band minimum along the X direction is folded back into the Γ point when the superlattice period is about 10 monolayers of Si. From [1]

beam epitaxy [1] led impetus to this concept, which was revisited by *Jackson* and *People* [41] in 1986 and, subsequently, by a number of other theoreticians. The essence of the idea is conveyed in Fig. 4. The new superlattice periodicity d along the growth direction results in a smaller Brillouin zone of size $\pm\pi/d$ compared with that of the original lattice ($\pm 2\pi/a$, where a is the lattice constant). The electronic band structure is then folded back into this new reduced Brillouin zone. For this simple model, it is apparent that the minimum in the conduction band in bulk Si is folded into the Brillouin zone center for $d \approx 5a/2$, which corresponds to 10 monolayers of Si, and a direct gap is evident. It is relevant that the superlattice zone folding occurs only along the growth direction and, in practice, strains within a Si_mGe_n superlattice together with the band offsets at the heterointerfaces compromise this naive picture (see, for example [1] and [42,43,44,45]). Theory has shown that for certain superlattice periods and when the Si layers are strained a direct energy gap is expected in Si_mGe_n superlattices, but the transition probability is still several orders of magnitude below that of GaAs because the electronic properties of the band-edge states are not sensibly modified by the zone-folding.

The first experimental evidence of modifications to the Si and Ge band structures in such superlattices was obtained from electroreflectance measurements of Si_4Ge_4 superlattices grown on (001) Si [46]. However, it was not until later on when strain-symmetrized Si_mGe_n superlattices were grown on strain-relaxed thick $Si_{1-x}Ge_x$ alloy buffer layers on Si that first indications of the predicted photoluminescence (PL) intensity enhancement and reduced

energy gap were obtained [1, 47]. Improvements in crystal growth conditions subsequently led to a positive identification of these new features [48]. Further details on the work on band-gaps and light emission in Si/Ge atomic layer structures are given in the review by *Abstreiter* [49].

Although infrared emission can readily be obtained at low temperature from such Si_mGe_n structures at energies useful for fiber-optic transmission work, the PL and electroluminescence (EL) is essentially quenched at room temperature due to exciton dissociation [50, 51]. Some promising steps towards room temperature EL structures have been reported [52, 53] and the development of undulating or wavy Si/Ge superlattice structures has allowed considerable improvements in PL tunability in the wavelength range 1.3 μm–1.55 μm combined with greater mechanical stability [49,54]. Nevertheless, the infrared emission is still weak and more recent results for Si/Ge wavy superlattice p–i–n diodes report an internal quantum efficiency of only $\sim 10^{-5}$ at 300 K [55]. Thus, from a device point of view, unless there are further major improvements in material quality it is most likely that these atomic layer superlattices will find eventual use as infrared detectors rather than as emitters [56, 57].

Quantum cascade and Terahertz (THz) emission structures both utilize Si/Ge superlattices, but they employ intraband transitions rather than the interband transitions of interest here and will be discussed later in Sect. 7.

3.2 Band Structure Engineering via Alloying

Alloying of Ge or C with Si allows engineering of the electronic band structure, where the energy gap may be varied with alloy composition and strain [57,58]. This is shown, for example, in Fig. 5 for strained $Si_{1-x}Ge_x$ on Si, where the tunability range is appropriate for fiber optic communications. Unfortunately, because of heterostructure stability limitations, the $Si_{1-x}Ge_x$ layer thickness must be kept below the critical thickness, which is defined as the maximum thickness for defect-free strained growth of the layer. Larger thicknesses imply relaxation of the layer due to the formation of dislocations and other lattice defects. The $Si_{1-x}Ge_x$ critical thickness decreases rapidly with increasing x (see Fig. 5). Thus the absorbing/emitting regions in infrared detectors/emitters are necessarily thin, although wavy $Si_{1-x}Ge_x$/Si superlattice structures may alleviate this restriction [54]. Also, and most significantly, the band-gap remains indirect. Despite these severe limitations much research has been carried out on the optical properties of $Si/Si_{1-x}Ge_x$ heterostructures [57], which exhibit type I band alignment [58,59], and, to a lesser extent, on $Si/Si_{1-x}C_x$ or even $Si/Si_{1-x-y}Ge_xC_y$ [60, 61, 62, 63].

Electroluminescence and PL have been observed from $Si_{1-x}Ge_x$ in both single layer and superlattice form with increased intensity compared with Si. The luminescence energy tracks the alloy composition dependence shown in Fig. 5, but at a lower energy [64, 65, 66, 67]. The recombination mechanism varies depending on the alloy layer thickness and crystalline quality, resulting

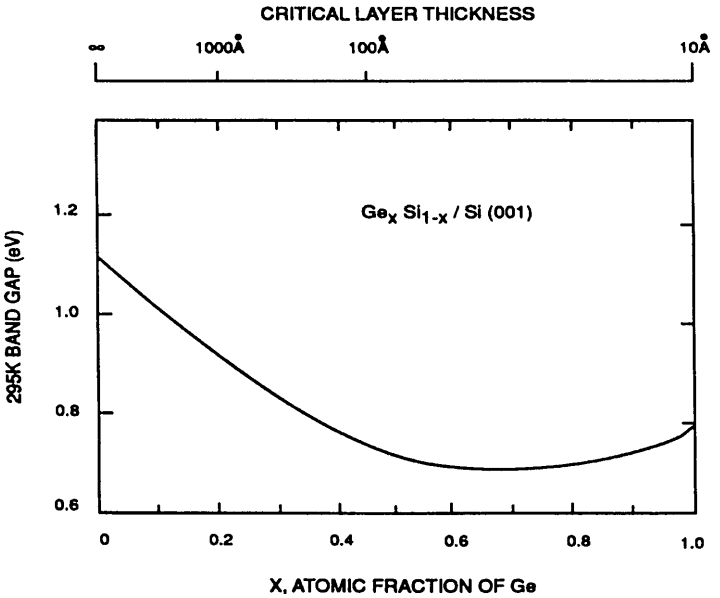

Fig. 5. The band-gap at room temperature of strained $Si_{1-x}Ge_x$ on Si. Also shown is the critical layer thickness as a function of x. From [57]

in near band edge and/or excitonic luminescence [68, 69, 70]. In the earliest work, the EL from $Si_{1-x}Ge_x$/Si p–n diodes was quenched by increasing the temperature above 80 K [64], but EL was soon reported at temperatures up to 220 K in p–i–n diode structures [71]. Progress in materials quality and device design has continued to improve EL device performance (see, for example, [72, 73, 74, 75, 76]) such that room temperature EL has now been reported at wavelengths near 1.3 μm [72, 76]. The major problem with such devices for practical purposes at present is their low efficiency at room temperature, which is again due to exciton thermal dissociation [72, 76]. For example, $Si_{1-x}Ge_x$/Si p–i–n diodes, which were grown on patterned substrates to optimize the unrelaxed alloy layer thickness [77], resulted in an internal quantum efficiency of just $\sim 10^{-4}$ for the EL at 300 K [55].

By alloying C with $Si_{1-x}Ge_x$ it was hoped that the compressive strain in $Si_{1-x}Ge_x$ layers on Si would be offset by the tensile strain exhibited by $Si_{1-x}C_x$ layers on Si and thereby permit relatively thicker strained alloy layers on Si with an improved conduction band offset [63]. Indeed, such strain compensation does occur in $Si_{1-x-y}Ge_xC_y$ layers on Si, but the range of compensation is limited by the low solubility of C in Si and also the small size of the C atom introduces severe distortions in the Si lattice near C sites. In addition, the alloy retains an indirect band-gap and only weak PL is obtained [60]. Much more work remains to be done on this ternary alloy system before its advantages over $Si_{1-x}Ge_x$ can be exploited.

4 Quantum Confinement

Research on the quantum confinement of carriers in silicon-based nanostructures including porous silicon (PS), nanoclusters, and quantum wells, wires, and dots forms a large part of the work on light emission in Si. Much of this work was stimulated by the discovery of bright visible light emission at room temperature in PS reported in 1990 [78]. The interest in nanostructures of Si stems from the effects of confinement on carrier wave functions when the crystallite diameter is less than the size of the free exciton Bohr radius of 4.3 nm in bulk c-Si [39]. The quantum confinement increases the electron–hole wave function overlap, resulting in increased light emission efficiency, and shifts the emission peak to higher energy [33, 79]. In addition, the probability of finding a non-radiative recombination center in these Si quantum dots decreases rapidly with decreasing dot size. When a non-radiative recombination center is present in the dot, exciton recombine non-radiatively and the dot is dark with respect to luminescence. When there is no non-radiative recombination center, the dot is bright and the excited carriers recombine radiatively (i.e., the single dot has almost a 100% quantum efficiency). It is the statistical distribution of dark and bright dots that then determines the overall luminescence efficiency. Last but not least, the fact that the Si dots are usually formed in a dielectric matrix having a lower refractive index than that of c-Si increases the extraction efficiency of the light generated in the active material itself.

4.1 Porous Silicon

Porous silicon was discovered over 35 years ago by *Uhlir* [80]. The porous material is created by a partial electrochemical dissolution of Si wafers in HF-based electrolytes. Hydrofluoric acid, on its own, etches single-crystal Si extremely slowly, at a rate of only nanometers per hour. However, passing an electric current between the acid electrolyte and the Si sample speeds up the process considerably, leaving an array of deep narrow pores. Pores with diameters from nanometers up to micrometers and micrometers deep have been achieved both in disordered or ordered arrangements under specific etching conditions (see Fig. 6).

In July 1989, *Canham* conceived the idea of fabricating Si quantum wires in PS by reverting to the much slower chemical HF etch after electrochemically etching c-Si. In this way Canham proposed to join up the pores, leaving behind an irregular array of undulating freestanding pillars of c-Si only a few nanometers wide. In 1990, *Canham* [78] observed intense visible PL at room temperature from PS that had been etched under carefully controlled conditions. Visible luminescence ranging from green to red in color was soon reported for other PS samples and ascribed to quantum size effects in wires of width ~ 3 nm [78, 81]. Independently, *Lehmann* and *Gösele* [82] reported on the optical absorption properties of PS. They observed a shift

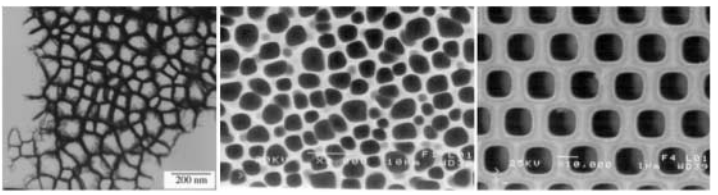

Fig. 6. Various images of PS samples obtained under different etching conditions. Pore sizes (from *left* to *right*) vary from some 100 nm to several micrometers and to 1 μm when arranged in an ordered array

in the bulk Si absorption edge to values as high as 1.76 eV that they also attributed to quantum wire formation. Tremendous activity on research into the physical and associated chemical characteristics of PS has ensued from these early reports. It is impossible to mention all of this work here and interested readers are directed to a number of reviews and books about PS [83, 84, 85, 86, 87, 88, 89, 90, 91, 92, 93, 94, 95, 96] for further aspects of this work.

The most widely studied PL occurs in the far-red to orange-yellow wavelength region, which we shall denote simply as the "red" PL. Interest in red PL stems from the fact that it is the only one that can be electrically excited. This PL shifts to shorter wavelength with increasing chemical dissolution time or increasing anodization current density. It was soon found that much smaller immersion times were required to produce noticeable blue shifts when the chemical dissolution was carried out in the presence of light. The spectra also show a blue shift with increasing anodization current density. As the porosity (defined as the void density) of PS increases with increasing anodization current density, the behavior of the red PL spectra qualitatively reflects the differences in sample porosity and hence in the dimensions of Si nanocrystals within PS (a larger void density is associated with a smaller c-Si skeleton size). The blue shift of the PL and optical absorption with increasing porosity provided the first important evidence that quantum confinement plays a significant role in PS, which has since been confirmed by the observation of the splitting of the luminescent states, the polarization of the PL, and the phonon replicas seen in the PL under resonant excitation [95]. The dynamics of the emission is characterized by a room temperature decay of hundred of microseconds, while lifetimes of some milliseconds were observed at low temperature. The temperature evolution of the lifetimes has been interpreted as due to a thermal balance between dipole allowed recombination from higher energy singlet states and dipole forbidden recombination from lower energy triplet states. The PL peak wavelength and intensity are sensitive to the surface chemistry of PS, particularly with regard to the relative amounts of hydrogen and oxygen on the surface. Thus, besides the quantum confinement mechanism, various surface state and defect models have been invoked to explain the various other results obtained [85, 95, 97].

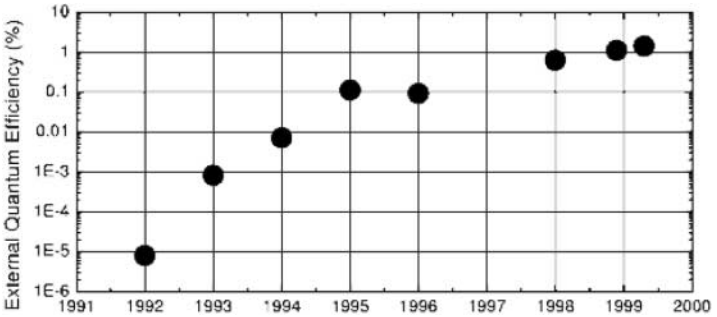

Fig. 7. External quantum efficiency of porous silicon LEDs over the years. The record in efficiency to date is that of [22]

Oxidation of the PS surface has been shown to produce blue PL [85]. The blue PL is quite weak in as-prepared PS, becomes intense only after strong oxidation and has a nanosecond decay time. Models currently under consideration include band-to-band recombination in Si nanocrystals, emission from oxide, and emission due to surface states [96].

Blue PL has been observed also in oxide-free PS simply by decreasing the size of the Si crystallites in accordance with the quantum confinement mechanism [97, 98]. In fact, the PL can be tuned from the c-Si band-gap of 1.1 eV all the way up to $\sim$ 3 eV by a judicious choice of the porosity in unoxidized PS [97, 98, 99].

The near-infrared PL [85] at $\sim$ 0.8 eV (below the bulk Si band-gap) exhibits complex nonexponential dynamics, with a wide distribution of decay times, and has been assigned to deep level transitions associated with dangling bonds on the surface of the Si nanocrystals [100].

From these considerations it is apparent that PL in PS is very sensitive to the chemistry of PS production and treatment. Si wires or nanocrystals and amorphous Si (a-Si) material, or any combination of them, may be formed in a given sample. The PS layers thus formed may be far from uniform, which adds to the difficulties in analyzing their optical properties. Other light emitting species may also be formed on the surfaces of the anodized and otherwise chemically treated Si.

Despite all these disadvantages, the ease of production of PS and the facts that the room temperature PL is very efficient (1%–10% external quantum efficiency [93, 94]) and that it is tunable through blue to near infrared wavelengths have led to impressive efforts to produce practical room-temperature devices. The evolution of PS LED performance over the years is reported in Fig. 5 [22]. The PS approach has, however, a draw-back in the high reactivity of the sponge-like texture, which causes rapid ageing of the LED and uncontrollable variations of the LED performances with time [96]. This major disadvantage has recently been overcome with an appropriate passivation of the PS surface although at the cost of a lower LED efficiency [101].

The latest red LEDs have exhibited external quantum efficiencies greater than 1% and lifetimes of the order of months [22, 102]. Such LEDs have been integrated into Si microelectronic circuits to provide an addressable LED display [103]. However, improvements in efficiency and power dissipation are necessary for display applications, while an increased modulation frequency (presently $\sim 1\,\mathrm{MHz}$ [104]) is required for optical interconnects. One way to improve the EL efficiency, to narrow the band width, to improve the directionality, and to increase the long-term stability is to insert the LED into a PS resonant cavity [105]. Even so, the long switching times observed in present PS LEDs may yet prove to be an Achilles' heel in optoelectronic applications.

A large optically induced absorption change has been observed in PS [106]. This phenomenon has been used to form all-optical logic gates in PS and raises the possibility of fabricating all-optical integrated circuits on Si [86, 106, 107].

PS can be also applied to the formation of complex dielectric structures. The facts that during the etching the current density determines the porosity of the etched layer, that the refractive index of a layer is proportional to its porosity, and that the etching process occurs only at the pore tips, allow changing the refractive index of PS simply by changing the current density during the etching. A temporal current profile is reflected in a correlated in-depth refractive index profile. This allows the formation of dielectric multilayers such as Bragg reflectors or microcavities [108, 109], or the study of photon propagation in complex dielectric structures where the analogies between photons and electrons can be investigated [110] and new one-dimensional devices could be designed, e.g., an optical delay line.

If a crystal has uniaxial symmetry, the optical response of the lattice is characterized by two distinct values of the refractive index. A crystal possessing such anisotropic dielectric properties is said to be birefringent. In PS the optical anisotropy is due to the anisotropic geometry of the pores. The anisotropy of PS depends on the crystalline orientation of the silicon substrate. Birefringence has been reported in (100), (111), and (110) oriented PS [111, 112, 113, 114, 115]. In all these cases, the PS layer can be assumed to be uniaxial, and the direction of the optical axis to be normal to the surface for the (100) and (111) cases, and parallel to the surface for the (110) case. The birefringence of (100) oriented PS has been reported to be positive [111, 112, 113] and values of the order of 10% have been demonstrated [116]. This high birefringence has led to the development of polarizers, polarization-sensitive Bragg reflectors, and microcavity resonators based on multilayers of optically nanostructured silicon where their optical response is governed by a three-dimensional (in-plane and in-depth) variation of the refractive index.

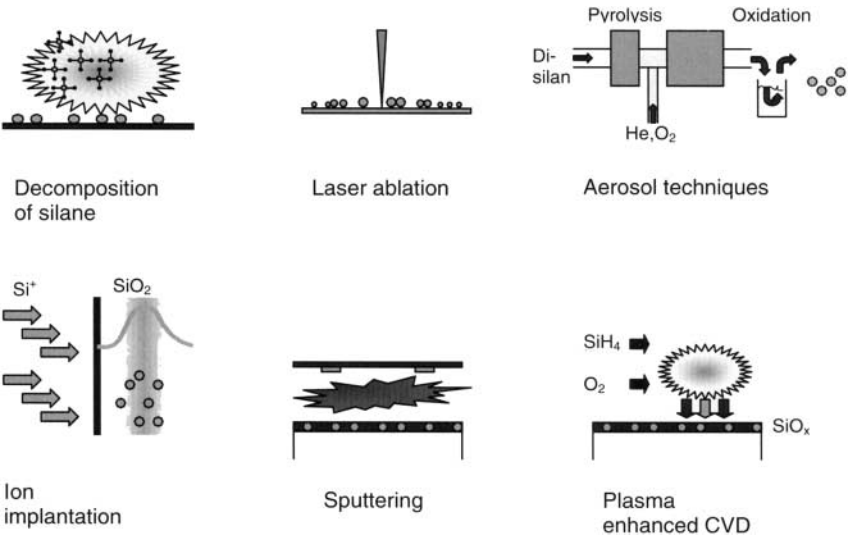

Fig. 8. Silicon nanocrystal fabrication techniques. The three lower techniques produce nanocrystals in a SiO_2 matrix. After [124]

4.2 Silicon Nanocrystals

Rather than produce nanometer-size Si crystals by etching, as in PS, there have been numerous attempts at growing them either directly from a gas phase or indirectly by recrystallization within a matrix (see Fig. 8) [33, 39, 117, 118, 119]. A popular approach is to produce Si nanocrystals (Si-nc) in a silica matrix to exploit the quality and stability of the SiO_2/Si interface and the improved emission properties of quantum confined Si. Many different approaches have been proposed to form the Si-nc [120, 121]. The most widely used are based on the deposition of sub-stoichiometric silica films, with a large excess of Si, followed by a high temperature annealing [122]. The annealing causes a phase separation between the two constituent phases, i.e., Si and SiO_2, with the formation of small Si-nc. The size and density of the Si-nc can be controlled by the deposition and the annealing parameters. Recently, the annealing of amorphous Si/SiO_2 superlattices has been proposed to control the size distribution and an almost monodispersed size distribution has been demonstrated [123].

It is noteworthy that the observation of a nanoparticle-size dependence of the PL energy in small Si-nc passivated with hydrogen [125] predates the similar finding in PS [78]. *Takagi* et al. [125] found that the PL peak energy varied as $1/d^2 (3 \leq d \leq 5\,\text{nm})$, where d is the Si nanocrystal diameter, in accordance with quantum confinement effects predicted by a simple effective mass model. As for PS, however, the emitted light energy generally falls below that expected from calculations of the energy gap for Si spheres [85]. Also, the confinement effect is seen [125, 126, 127] or not seen [128] in emission de-

pending on sample preparation. Interpretation of the nanocrystal PL spectra suffers from the same ambiguities as PS, i.e., nanocrystal size distribution effects and surface chemistry effects [119]. Quite surprisingly, single nanocrystal luminescence experiments show a linewidth of the emission spectra of some hundreds of meV [129], which could suggest either a strong vibronic character of the emission or that recombination is not due to quantum confinement but is related to surface state emission. Indeed, the nanocrystal structure may deviate from the cubic diamond structure for very small Si nanoclusters [33]. Calculations [130, 131] have shown that luminescence in Si-nc can be due to excitons trapped at the surface, which is passivated by hydrogen or silicon oxide, while the optical absorption is characteristic of quantum confinement effects. In addition, localized radiative levels can be formed at the Si-nc interface due to the presence of the Si=O (silanone) double bond. First principle calculations show that multiple Si=O defect centers could form on the Si-nc surface and that the emission energy does not shift appreciably as the number of defects increases [132]. The red PL quantum efficiency and lifetime is similar to that found for PS [133], indicating a similar light emission mechanism involving quantum-confined nanocrystal states. The observation of phonon assisted optical transitions in oxidized Si nanocrystals has also been reported by *Kovalev* et al. [134] and they found that for confinement energies above 0.7 eV the radiative transitions are governed by no-phonon quasidirect processes. Direct measurements of the conduction and valence band edges of Si nanocrystals with diameters from 1 to 5 nm using X-ray absorption and photoemission spectra have confirmed the quantum size effect in the band structure [135], although the increase of the band-gap with decreasing nanocrystal size is lower overall than that predicted by theory. The role of the surface is, however, a key factor in the interpretation of the emission mechanism [136]. Thus, the vagaries and complexities of the nanocrystal-interface-surface system are still proving difficult to unravel.

Nanocrystals of Si embedded in dielectrics form an attractive system for device fabrication when compared with PS, because of the increased surface stability and material rigidity. Visible electroluminescence (EL) has been observed, for example, from Si-nc embedded in films of a-Si:H [137] and from an electrochemically-formed nanocrystalline Si thin film deposited on SnO_2 [138]. In the latter case the p–i–n LED at room temperature emitted orange-red light (1.8 eV) that was readily visible to the eye. The light emission is ascribed variously to near surface states [137] and the quantum size effect [138]. Also, infrared emission near 1.1 eV has been obtained from a room-temperature EL device comprised of Si-nc embedded within a Si-rich SiO_{2-x} matrix [139]. The EL from this structure has an external quantum efficiency of 10^{-3} [140].

The refractive index of Si-nc is larger than the one of SiO_2, thus high quality waveguides can be prepared [141]. In such systems optical gain has

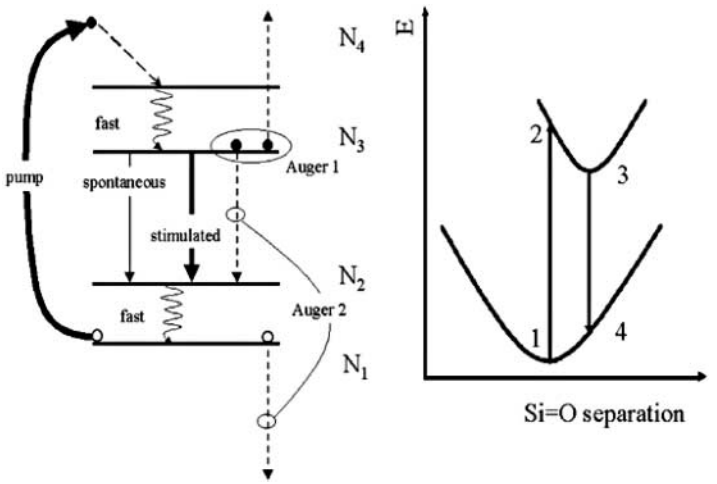

Fig. 9. (*Left*): An effective four level system that has been introduced to model qualitatively the recombination dynamics under gain conditions. From Level 3 the excited carriers can recombine by spontaneous, stimulated, or Auger recombinations. (*Right*): Schematic of the energy configuration diagram of the silicon-nc in an oxygen rich matrix. Localized radiative states are formed inside the nanocrystal band-gap by the interface oxygen atoms. The excited nanocrystal state can occur at a different lattice coordinate than that of the ground state. From [149]

been observed [121, 142, 143, 144, 145, 146, 147, 148, 149] by using various complementary techniques:

- a superlinear increase of the luminescence intensity as a function of the pumping rate [121, 146],
- amplified spontaneous emission in a waveguide geometry [142, 143, 144, 147, 148, 149],
- probe amplification in transmission experiments under high pumping excitation [142],
- collimated and speckled patterned emissions, which show the coherent properties of the emitted light [146], and
- an increase of the degree of polarization as a function of the pumping rate [150].

Some concerns have been raised about the methods used to measure the gain [151], and other studies have failed to observe light amplification in pump and probe experiments [152]. Here it seems that the main problem is related to the measurement techniques, which although easy in principle have many subtleties that should be considered [153]. Almost all of the authors agree on the fact that the gain is due to localized state recombinations either in the form of silicon dimers or in the form of silanone Si=O bonds created at the interface between the Si-nc and the oxide or within the oxide matrix. The

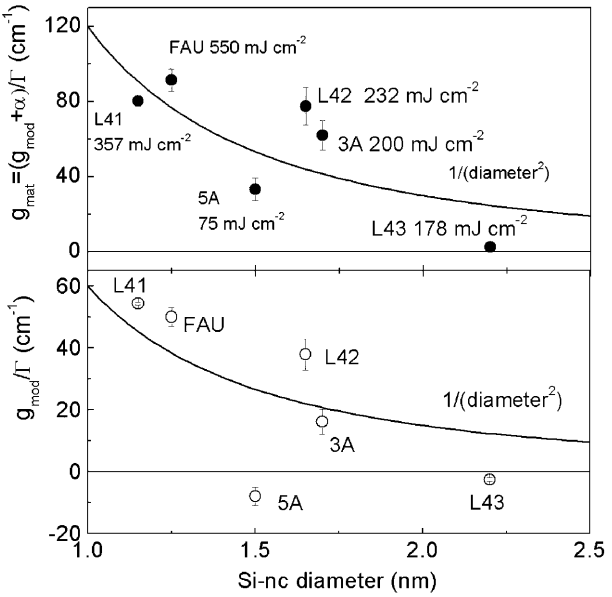

Fig. 10. Modal gain and material gain measured under pulsed conditions (on each data point the fluency is reported under pump conditions of 355 nm, 6 ns, and 10 Hz) for various Si-nc waveguides as a function of the Si-nc diameter. Here, L41, L42, and L43 refer to samples grown at MPI-Halle (Germany) by a size-controlled deposition technique [123], 5A and 3A to samples grown by PECVD in Catania (Italy) [154], and FAU to samples grown in Rochester (USA) [155]. The bottom plot is the net gain obtained by the measured gain coefficient g_{mod} divided by the optical mode overlap with the Si-nc rich layer (optical mode confinement factor Γ). The upper plot refers to the estimated material gain g_{mat} which takes into account the propagation losses α measured at the same wavelength as the gain measurements under CW measurements

suggested scheme to explain population inversion and, hence gain, is a four level model where a large lattice relaxation of the photoexcited localized center gives rise to the four levels (see Fig. 9) [143, 149].

From Fig. 9 it is clear that stimulated emission is competing with other non-radiative recombination mechanisms such as Auger or excited state absorption. In particular, time resolved experiments on the amplified spontaneous emission from Si-nc in a waveguide geometry [143, 144, 149] have shown an extremely fast component (nanosecond lifetime) due to stimulated emission. A delicate interplay between Auger recombination and stimulated emission governs the possibility of observing optical gain in Si-nc. As discussed in [149], the Si-nc density should be large enough to yield a significant optical gain.

Figure 10 shows a summary of various experimental results obtained in Trento University on various samples prepared using different methods. It is

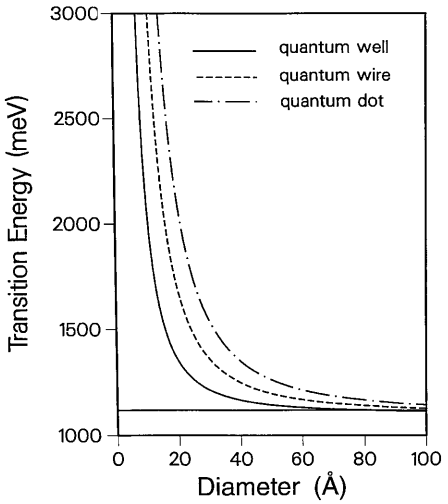

Fig. 11. Optical gap in Si quantum wells, wires, and dots versus system diameter. The transition energy is calculated for the lowest electron and heavy hole energies for infinite confining potentials. From [161]

interesting to note that, in addition to the packing density, another parameter governs the possibility and strength of material gain, i.e., the Si-nc size. As the Si-nc size decreases the material gain increases, and maximum gain values of $100\,\mathrm{cm}^{-1}$ under pulsed excitation are reported in the figure.

The problem of gain in Si-nc still has some unanswered queries: 1. what is the role played by the Si-nc and by the embedding medium, 2. what are the key parameters that determine the presence of gain in the Si-nc, 3. how is the nanocrystal interaction influencing the gain, and 4. what is the precise nature of the four levels in the model and, in particular, the location and role of Si-O bonds. Substantial progress in the development of such nanocrystalline-Si structures exhibiting optical gain can be expected over the next few years.

The Si-nc system is a very promising one in which to achieve a laser. Indeed, all the other key ingredients for a laser have been demonstrated. Vertical optical microcavities based on a Fabry–Pérot structure with mirrors constituted by distributed Bragg reflectors (DBR) and where the central layer is formed by Si-nc dispersed in SiO_2 have been already fabricated [156]. The presence of a thick SiO_2 layer needed to form the DBR can be a problem for electrical injection when current has to flow through the DBR. Lateral injection schemes can avoid these problems. On the other hand, electrical injection into the Si-nc is a delicate task in itself [157]. Bipolar injection is extremely difficult to achieve. Despite some claims, most of the reported Si-nc LEDs are impact ionization devices: electron–hole pairs are generated by impact ionization via the energetic free carriers injected through the electrode. By exploiting impact ionization, Si-nc LEDs have been demonstrated with EL spectra overlapping PL spectra, an onset-voltage as low as 5 V, and efficiencies in excess of 0.1% [158]. Some unconfirmed claims of near-laser action of Si-nc LEDs have appeared in the literature [159, 160].

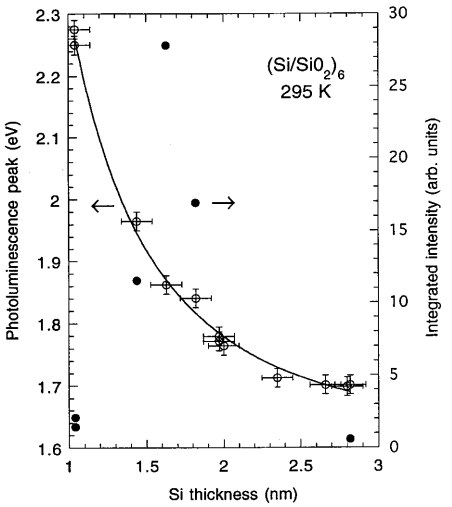

Fig. 12. The PL peak energy (*open circles*) and integrated intensity (*filled circles*) at room temperature in $(Si/SiO_2)_6$ superlattices as a function of Si layer thickness. The *solid line* is a fit with effective mass theory. From [167]

4.3 Quantum Wells, Wires and Dots

One of the major problems involved in PS and Si-nanocluster research and development work is the inhomogeneity of the material. Such inhomogeneous broadening effects in the PL and EL can be minimized by preparing *uniform* Si structures in the form of quantum wells, wires, or dots. Such structures can readily be produced directly by modern epitaxial growth techniques such as planar epitaxy, quantum wire formation along wafer steps, and dot self assembly, or indirectly by etching appropriate planar structures in the case of wires and dots. The predicted Si transition energies [161] due to the different degrees of quantum confinement are shown in Fig. 11 (more sophisticated pseudopotential calculations [162] give qualitatively similar results), where it can be seen that appreciable confinement effects are seen only for diameters less than 3 nm. Etched structures of this size have been difficult to produce in Si until recently.

4.3.1 Wells

The simplest approach is to grow thin quantum wells of Si separated by wide band-gap barriers. Suitable barrier candidates are SiO_2, CaF_2, and Al_2O_3 [163], and SiO_2 has the additional advantage of being an excellent passivator of Si [164]. Although a number of Si/barrier superlattices have been produced in the past [165] none has produced convincing evidence for quantum confinement induced emission until recently. In 1995, *Lu* et al. [166] reported visible light emission at room temperature from ultra thin-layer Si/SiO_2 superlattices grown by molecular beam epitaxy (MBE) that exhibited a clear quantum confinement shift with Si layer thickness, as shown in Fig. 12. The indications of direct band-to-band recombination were confirmed

by measurements via X-ray techniques of the conduction and valence band shifts with layer thickness [166, 168]. The integrated intensity at first rises sharply with decreasing Si thickness until $d \approx 1.5\,\text{nm}$ and then decreases again, which is consistent with quantum well exciton emission [169,170]. The PL intensity is enhanced by factors of up to 100 on annealing and is also selectively enhanced and band-width narrowed by incorporation into an optical microcavity [171, 172]. Such superlattices have now been produced in an industrial environment [173]. The Si quantum wells in these superlattices have a disordered, but nearly crystalline, structure. Recently, the confinement effects have been reproduced in single ultra-thin c-Si wells formed from industrially produced Si-on-insulator wafers [174].

Theoretical calculations of the optical properties of Si/SiO_2 superlattices based on an empirical pseudopotential homojunction model [175] revealed that for Si layers in the (100) direction the energy gap is pseudodirect, i.e., the optical transition matrix element is smaller than that of a direct transition as in bulk GaAs. Nevertheless, the energy increases with decreasing Si quantum-well thickness and the transition matrix element increases steeply up to $\sim 2\,\text{nm}$ thickness and then decreases again in general agreement with the experimental results given in Fig. 12. Tight binding band structure calculations for $Si_m/(SiO_2)_n$ crystalline superlattices with the number of unit cells $m, n \leq 5$ [176] show a striking new feature. Besides the expected increase in the band-gap due to quantum confinement, the confined bands along the Γ–Z symmetry direction are essentially dispersionless and exhibit a strongly-nested direct band-gap character at the minimum energy gap of the system. Thus, these superlattices produce a high radiative efficiency for a 1 nm–3 nm ($m = 2$–5) Si layer thickness [176], as found experimentally.

The bright PL obtained from as-grown and annealed Si/SiO_2 superlattices offers interesting prospects for the fabrication of a Si-based light emitter that can be tuned from 500 to beyond 800 nm by varying the Si layer thickness and/or the annealing conditions, all using available vacuum deposition technology and standard Si wafer processing techniques. The next important step is to develop LEDs based on such superlattices. Several prototype devices have been constructed in Si/SiO_2 [177,178,179,180,181] and all report visible EL, although as yet there is no strong evidence that the emission originates from confined states in the Si quantum wells. The EL from the Si/SiO_2 superlattices is notably stable [177,178]. An optically active microcavity with a Si/SiO_2 superlattice inserted in the cavity has also been realized [182].

4.3.2 Wires

Quantum wires obtained by etching $Si/Si_{1-x}Ge_x$ heterostructures have been investigated by several groups (see, for example, [183] and [184]). In PL measurements, wires defined by electron beam lithography and reactive ion etching have shown small blue shifts of up to 30 meV in the $Si_{1-x}Ge_x$ alloy peak at $\sim 1.1\,\text{eV}$ due to a combination of strain and confinement [183, 184].

Alternatively, $Si_{1-x}Ge_x$ wires have been grown on V-groove patterned Si substrates [185]: The infrared emission (PL and EL) in this case exhibits a large optical anisotropy [186]. No significant intensity enhancements compared with PL from quantum well transitions have been realized in these wire structures.

Until recently, it has not been possible to produce thin enough freestanding wires of c-Si by etching techniques to observe quantum confinement effects, although room temperature PL at wavelengths from 400 nm–850 nm is found for pillars with diameters $\sim$ 10 nm (see, for example, [187, 188, 189] and references therein). Recently, an EL device based on such Si nanopillars has been produced: The device emitted red light that was visible to the naked eye [190]. New etching techniques have now been developed for fabricating Si quantum wires with dimensions in the sub-10-nm region that after thermal oxidation should allow investigation of the optical properties of sub-2-nm wires in conventional wire [191] and free-standing pillar [192] form. Two-dimensional lattices of Si nanopillars have been shown to exhibit photonic band-gap properties that can be extended to submicrometer wavelengths [193]. Owing to the huge free space within these photonic crystals, luminescent materials may be readily incorporated to produce a photonic-band-edge laser.

In alternative production methods, Si nanowires have also been synthesized directly [194, 195]. Although the wire diameters obtained so far ($\sim$ 10 nm–30 nm) are too large for the observation of carrier confinement [196], these nanowires [197] and also Si nanoparticle chains [198] exhibit interesting electron field emission properties. Confinement effects could be induced in these wires by using thermal oxidation to reduce the Si nanowire diameter [195].

Theoretical calculations of the electronic structure and optical properties of H-passivated Si quantum wires have been reported by a number of research groups (see, for example [199] and references therein). First principles calculations show the same band nesting phenomenon and near-flat dispersion along the Γ–Z symmetry (wire) direction, as described above for Si quantum wells, and the occurrence of direct gaps [199, 200].

4.3.3 Dots

Attention has now turned mainly to the production of Si and $Si_{1-x}Ge_x$ quantum dots, in addition to the Si/SiO_2 system. Quantum dots fabricated by etching $Si/Si_{1-x}Ge_x$ superlattices have produced 4 K PL at 0.97 eV that is 200 times brighter in 60 nm dots compared with the unetched superlattice PL [201]. Similar studies of $Si_{1-x}Ge_x$ dots fabricated by self-assembling island growth on Si have shown an increased luminescence efficiency due to the localization of excitons in the dots [202]. In the latter case, the dots were buried in Si, which has the advantage of minimizing surface defect recombination. In both cases, EL has been observed from diode structures at low

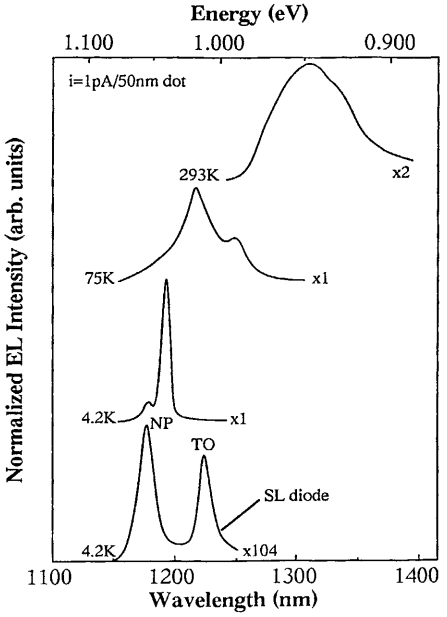

Fig. 13. Temperature dependence of EL spectra of a 50 nm $Si/Si_{0.7}Ge_{0.3}$ quantum dot diode under reverse bias of 0.5 V and an injection current of 1 pA/dot. A reference spectrum from a superlattice (SL) diode is also shown. After [203]

temperatures [202, 203] and at room temperature [203], as shown in Fig. 13. The infrared EL at 4.2 K in the dot is two orders of magnitude higher in intensity than in the as-grown superlattice (see Fig. 13). At room temperature, the dot EL at 1.3 μm is only 50% less efficient, with a threshold injection current of $\sim$ 0.1 pA/dot and an electrical-input to optical-output power conversion efficiency of 0.14% [203].

In subsequent work on Si quantum dots, $\sim$ 10 nm in size, formed in a-Si/SiO_2 superlattices by controlled Si crystallization, *Tsybeskov* et al. [204] have shown that the PL emitted near 1.1 eV is remarkably efficient ($\sim$ 0.2% external quantum efficiency at 300 K) compared with c-Si. The high efficiency is due to spatial confinement of carriers in well passivated pure Si dots. A shift of the PL peak toward higher energies was found with smaller-size ($<$ 10 nm) Si dots. Optical gain has since been measured in these Si dots [155, 205]. The PL in such dots can be tuned up in energy by confinement and down in energy by alloying of Ge with Si. The latter case has been investigated in MBE-grown $Si_{0.5}Ge_{0.5}$ dots in coherent-wave superlattice structures. Here, strong no-phonon PL was obtained at $\sim$ 0.8 eV (1.55 μm) that could easily be varied in wavelength by changing the Ge content [54].

5 Impurities

5.1 Luminescence via Impurity Centers in Silicon

Another approach to increasing the EL efficiency of an indirect band-gap semiconductor is to introduce an impurity that localizes the electron and hole, as pioneered in GaP [206]. This has been done in Si EL diodes by using, for example, rare earth impurities [207], carbon complexes [208], and sulfur/oxygen complexes [209] as localization centers for electron–hole recombination. Extrinsic luminescence in Si can arise from a variety of sources [37,38]. Here, we concentrate on isoelectronic and rare-earth extrinsic centers, as these are presently the most promising for optoelectronic device applications.

Isoelectronic centers are created by doping Si with electrically neutral impurities such as the isovalent elements C, Ge, and Sn or a multiple-atom complex with no dangling bonds. Isoelectronic impurities bind free excitons in Si, which can increase the probability of electron–hole recombination due to spatial confinement of the particles. The resultant recombination energy may appear as light or disappear through phonon generation and other nonradiative decay channels [33,210].

The optical properties of a variety of such isoelectronic impurity centers including In, Al–N, Be, S, and Se have been studied both in Si and $Si_{1-x}Ge_x$ alloys [33,38,210]. A luminescence external quantum efficiency of 5% and a lifetime greater than 1 ms have been reported for the S complex emission at 1.32 μm in Si at low temperatures [211], but the PL intensity and lifetime decrease sharply with increasing temperature. This variation with increasing temperature is due to exciton dissociation and competing nonradiative recombination processes. The low bound-exciton emission intensity at room temperature militates against isoelectronic-impurity based EL devices at present.

The optical properties of rare earth ions in solids have been investigated in great detail and are generally well understood [212]. The optical emission of the Er^{3+} ion is of particular interest for semiconductor device applications, because it occurs near 1.5 μm. The Er^{3+} ion emits photons at 1.54 μm in Si by intracenter transitions between Er^{3+}-ion discrete states ($I_{13/2} \rightarrow I_{15/2}$ transition within the 4f electron shell) [213]. The excitation of the Er^{3+} ions contained in Si is a complicated process [33,214,215] involving first electron–hole carrier generation in Si, then exciton formation, and finally Er excitation by an intracenter Auger process, with a number of competing pathways in the excitation process. High internal quantum efficiencies are observed when Er is surrounded by a strong electronegative ligand field, and room temperature EL devices with improved performance through the use of an oxygen codopant are emerging (see, for example [216,217,218,219,220]). The room temperature EL from Si coimplanted with Er and O is shown in Fig. 14. From such LED under reverse bias, an internal quantum efficiency of 0.05%, an emitted power

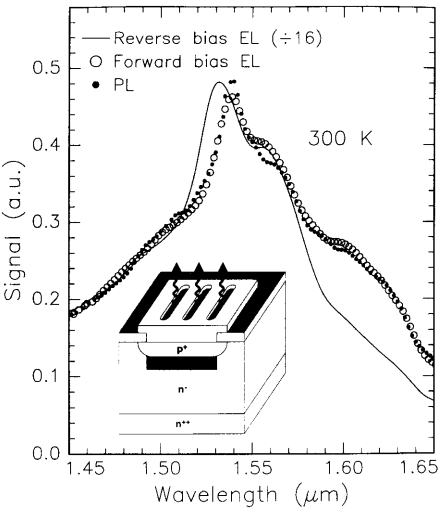

Fig. 14. Room-temperature EL spectra of Si:Er,O under reverse (*solid line*) and forward bias (o) conditions for a diode current density of 2.5 A/cm^2 compared with the PL (•). The *inset* gives a schematic of the LED structure. From [215]

of 0.2 mW, and a modulation frequency of 10 MHz have been achieved [215, 220].

5.2 Erbium Coupled with Silicon Nanocrystals

What it is more interesting for light amplification studies is the experimental finding of a strong enhancement of the Er luminescence when Er is implanted or deposited in a SiO_2 matrix where Si-nc have been formed, i.e., Si-nc acts as sensitizers for erbium ions [221, 222, 223]. Nonradiative de-excitation processes are reduced by widening the Si band-gap and thus avoiding one of the most detrimental sources of Er luminescence quenching. Indeed, the thermally activated back-transfer of excitation from Er^{3+} ions to Si-nc becomes less efficient than in bulk Si since the energy mismatch for the process becomes larger. Widening of the band-gap also produces a reduction in the free carrier concentration thus limiting the Auger processes. As demonstrated in Fig. 15, a strong luminescence comes from Er^{3+} ions that are pumped through an electron–hole mediated process in which photo-excited excitons from Si-nc transfer their energy to Er^{3+} ions [221, 222]. The number (between 1 to 10) of Si-nc coupled to a single Er^{3+} ion is still a debated issue [222, 224]. Regarding where Er is placed, from high resolution luminescence it is clear that most of the Er is in the SiO_2 matrix, which is an ideal situation for reproducing the environment that is found in an Er-doped fiber amplifier. Hence, Er coupled Si-nc has the advantages of both Si (efficient excitation) and SiO_2 (weak non-radiative processes, i.e., negligible temperature quenching of the luminescence), while it avoids their disadvantages (low excitation efficiency in SiO_2 and strong non-radiative processes in bulk Si). Indeed, MOS light-emitting devices operating at room temperature have been made with this system,

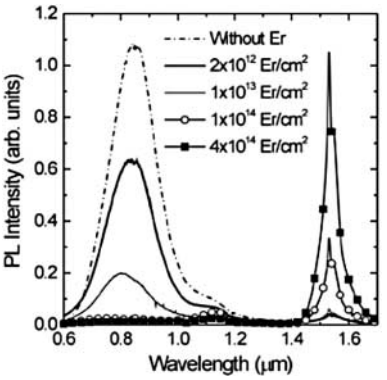

Fig. 15. Room temperature PL spectra of Er-implanted Si nanocrystals at different Er doses. The pump power of the laser beam was 50 mW. After [222]

and a quantum efficiency greater than 1% has been demonstrated [225]. Even higher efficiencies (10%) are reported for Er in silicon rich oxide films; however, in this system reliability is still an issue [226].

The layer co-doped with Si-nc and Er^{3+} ions has a refractive index that is larger that SiO_2, i.e., waveguides can be formed with a core containing Er^{3+} ions coupled to Si-nc. Experiments have shown that the luminescence intensity increases [227] or there is even evidence of signal enhancement [228] in these waveguides. Even though no net optical gain was measured, an enhancement in the probe transmission at 1.535 μm was observed as the pump power was increased. A fit to the experimental data yields an increased Er^{3+} ion emission cross section compared to Er^{3+} ions in silica or in Si [229]. This is a quite unexpected result, which conflicts with the observation of a millisecond lifetime from Er coupled Si-nc. The reason for the emission cross section increase is still unclear; one can speculate about the role of the dielectric environment, which is modified by the presence of the Si-nc [224]. What makes this finding interesting is the possibility to significantly reduce the cavity length in an amplifier or laser than the one usually employed in the Er-doped fiber systems. Sizeable gain can be further obtained by low Er doping concentrations. To summarize the very interesting properties of the Er^{3+} ion coupled Si-nc system, Table 1 compares the observed cross sections of Er^{3+} ions in silica, in Si, and coupled with Si-nc.

The system of Er^{3+} ions coupled with Si-nc is very promising for laser applications, because the active material (Er^{3+} ions in SiO_2) has already shown lasing properties. In addition, the technology to produce the material is very compatible with CMOS processing. Microcavities with excellent luminescence properties have been also demonstrated [156], which allows the design of both edge emitting or vertical emitting laser structures. The issue related to electrical pumping of the active material, which was believed to be a major draw-back of this approach, can be worked out since extremely high efficiency LEDs have been demonstrated [225, 226]. A still open issue is the ability to engineer waveguide losses in order to be able to measure net opti-

Table 1. Summary of the various cross sections related to Er^{3+} ions in various materials

	Er in SiO_2 (cm^2)	Er in Si (cm^2)	Er in Si-nc (cm^2)	Reference for Er in Si-nc
Effective excitation cross section of luminescence at a pumping energy of 488 nm	$(1–8) \times 10^{-21}$	3×10^{-15}	$(1.1–0.7) \times 10^{-16}$	[230, 231]
Effective excitation cross section of electroluminescence		4×10^{-14}	1×10^{-14} by impact ionization	[225]
Emission cross section at 1.535 µm	6×10^{-21}		2×10^{-19}	[229]
Absorption cross section at 1.535 µm	4×10^{-21}	2×10^{-20}	8×10^{-20}	[232]

cal gain and not only signal enhancement in pump and probe experiments. Further work should then be spent on optimizing the gain with respect to the waveguide parameters and developing a suitable optical cavity that can be electrically injected.

6 Photonic Components

It was predicted in the early 1990s that Si based optoelectronics will be a reality before the end of the century [9, 120]. Indeed, except for a Si-based laser, all the basic components have been already demonstrated [233], as outlined below and described in greater detail in the following chapters.

6.1 Silicon Based Waveguides

The first essential component in Si microphotonics is the medium through which light propagates: the waveguide. This has to be Si compatible and should withstand normal microelectronics processing. Critical parameters are the refractive index n of the core material, its electro-optical effects, the optical losses, and the transparency region. To realize low-loss optical waveguides, various approaches have been followed (see Fig. 16) [234]: low dielectric mismatch structures (e.g., doped silica [235], silicon nitride [236], silicon oxynitrides on oxide [237], or differently doped Si [238]) or high dielectric mismatch structures (e.g., Si on oxide [239]). Low loss silica waveguides are characterized by large dimensions, typically 50 µm thick, due to the low refractive index mismatch ($\Delta n = 0.1\%–0.75\%$). Silica waveguides have a large mode

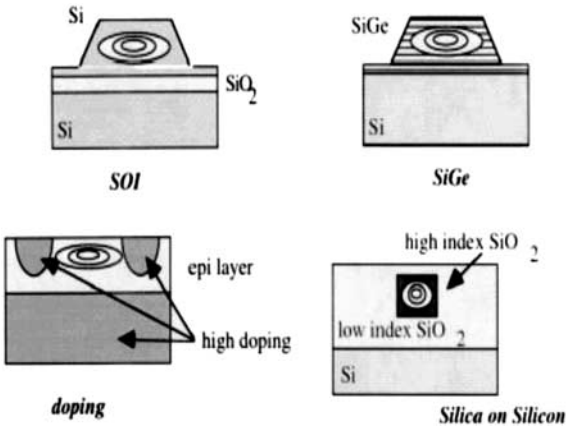

Fig. 16. Different approaches used for the fabrication of optical waveguides on Si substrates. From [233]

spatial extent and, thus, are interesting for coupling with optical fibers but not for integrating into/within electronic circuits because of their significant difference in sizes. The large waveguide size also prevents the integration of a large number of optical components in a single chip. Similar problems exist for Si on Si waveguides where the index difference is obtained by varying the doping density [238]. Si on Si waveguides are very effective for realizing free-carrier injection active devices (e.g., modulators) as well as fast thermo-optic switches owing to the high thermal conductivity of Si. A major problem with these waveguides is the large free carrier absorption, which causes optical losses of several dB/cm for single-mode waveguides at 1.55 μm. Silicon nitride based waveguides [236] and silicon oxynitrides waveguides [237] show losses lower than 0.5 dB/cm at 633 nm and bending radii of less than 200 μm. The nitride based waveguides are extremely flexible with respect to the wavelength of the signal light: both visible and IR.

At the other extreme, Si on insulator (SOI) or polysilicon-based waveguides allow for a large refractive index mismatch and, hence, for small size waveguides in the sub-micrometer range. This allows a large number of optical components to be integrated within a small area. Optical losses as low as 0.1 dB/cm at 1.55 μm have been reported for channel waveguides in SOI (optical mode cross-section $0.2 \times 4\ \mu m^2$) [240]. Ideal for on-chip transmission, SOI waveguides have coupling problems with silica optical fibers due to both the large size difference and the different optical impedance of the two systems. Various techniques have been proposed to solve these problems, among which are adiabatic tapers, V-grooves, and grating couplers [241,242]. Large single-mode stripe-loaded waveguides on SOI can be achieved provided that the stripe and slab are both made of Si [243]. This SOI system provides low loss waveguides (< 0.2 dB/cm) with single mode operation, large rib structures

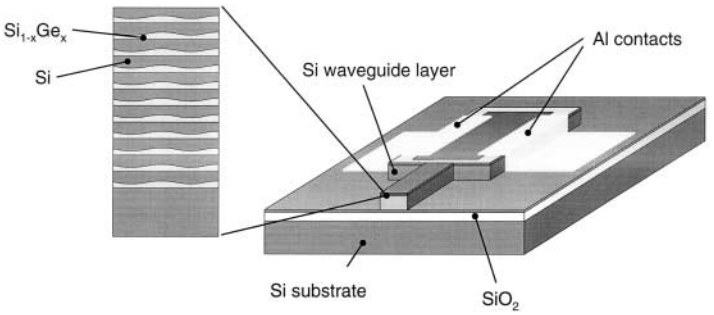

Fig. 17. Schematic representation of a $Si/Si_{0.5}Ge_{0.5}/Si$ waveguide photodetector based on a coherent wave $Si/Si_{0.5}Ge_{0.5}$ superlattice. The photocurrent quantum efficiency for the 240-mm-long waveguide detector was 0.1 A/W at 1.55 μm. (Source: S. Janz, National Research Council of Canada)

(optical mode cross-section $4.5 \times 4\,\mu m^2$), and low birefringence ($< 10^{-3}$). An appropriate geometry, with the use of an asymmetric waveguide, allows bend radii as short as 0.1 mm [244]. A number of photonic components in SOI have been demonstrated [243] and commercialized [244]: directional couplers, dense WDM arrayed waveguide gratings, Mach–Zehnder filters, Star couplers, etc.

6.2 Detectors

The optical signal is converted into an electrical signal by using Si based photodetectors. Detectors for Si photonics are based on three different approaches [245]: Si photoreceivers for wavelengths less than 1.1 μm, hybrid systems (mostly III–V on Si), and heterostructure based systems. High speed (up to 8 Gb/s) monolithically integrated Si photoreceivers at 850 nm have been fabricated by using 130-nm CMOS technology on a SOI wafer [246]. Other recent results confirm the ability of Si integrated photoreceivers to detect signals with a high responsivity of 0.46 A/W at 3.3 V for 845 nm light and a 2.5 Gb/s data rate [247]. The heterostructure approach is mainly based on the heterogrowth of Ge rich SiGe alloys: Ge-on-Si photodetectors have been reported with a responsivity of 0.89 A/W at 1.3 μm and a 50 ps response time [248]. A 1% quantum efficiency at 1.55 μm in a metal-semiconductor-metal (MSM) detector based on a Si/SiGe superlattice shows that promising developments are possible [249]. Similarly, waveguide photodetectors with Ge/Si self-assembled islands show responsivities of 0.25 mW at 1.55 μm with zero bias [250]. An example of a $Si/Si_{1-x}Ge_x$ waveguide photodetector is given in Fig. 17. The MSM detector is based on a $Si_{0.5}Ge_{0.5}/Si$ strained undulated superlattice and the waveguiding is provided by the SOI structure with SiO_2 and air cladding [251].

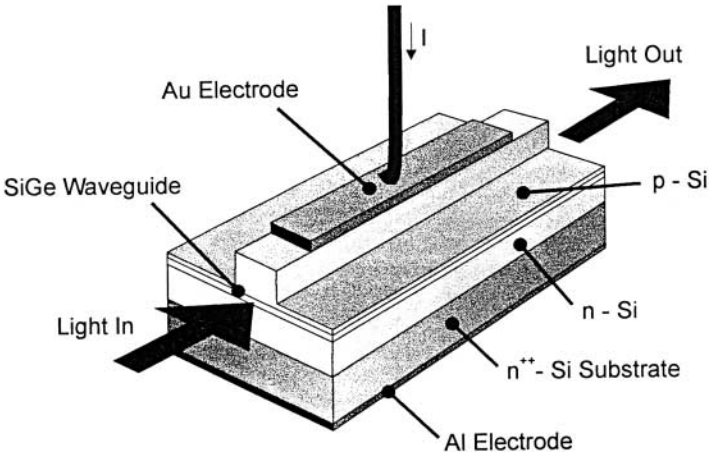

Fig. 18. Schematic representation of a $Si/Si_{0.85}Ge_{0.15}/Si$ p–i–n waveguide modulator. A maximum modulation depth of 66% was obtained at 1.3 μm for a 2-mm-long waveguide using a peak pulse current density of 2700 A/cm^2. After [253]

6.3 Other Photonic Components

Almost all the other required photonic components have been demonstrated in Si microphotonics [120, 245]. Optical modulators, optical routers, and optical switching systems have all been integrated into Si waveguides [252]. A discussion of a series of photonic component realized with SOI waveguides is reported in [243], including plasma-dispersion-effect based active gratings, evanescent waveguide coupled Si-Ge based photodetectors, and Bragg cavity resonant photodetectors. An example of a $Si/Si_{1-x}Ge_x$ photonic device is the rib-waveguide optical modulator shown in Fig. 18, where carrier injection in a $Si_{1-x}Ge_x$ p–i–n heterostructure allows optical intensity modulation in Si at megahertz frequencies [253]. Such monolithic modulators operating at much higher (gigahertz) frequencies are required in practice.

6.4 Silicon Photonic Integrated Circuits

Based on the technologies reported in the previous sections, various demonstrator models of photonic integrated circuits based on Si have been reported. Here we present some examples.

Hybrid integration of active components and silica-based planar ligthwave circuits provide a full scheme for photonic component integration within a chip [254]. Passive components are realized by using silica waveguides while active components are hybridized within the silica. Active components (laser diodes, semiconductor optical amplifiers, and photodiodes) are flip-chip bonded on Si terraces where also the optical waveguides are formed. By using this approach various photonic components have been integrated such as

multi wavelength light sources, optical wavelength selectors, wavelength converters, all optical time-division multiplexers, etc. [254]. Foreseen applications of this technology include WDM transceiver modules for fiber-to-the-home use.

A fully integrated optical system based on silicon oxynitrides waveguides, Si photodetectors, and CMOS transimpedance amplifiers has been realized [237]. Coupling of visible radiation to a Si photodetector can be achieved by using mirrors at the end of the waveguide. These are obtained by etching the end of the waveguide with an angle so that the light is reflected at almost 90 degrees into the underlying photodetector.

Commercial systems for the access network telecommunications market have been realized by using SOI waveguides and the Si optical bench (SOB) approach to interface the waveguides with both III–V laser sources and III–V photodetectors. The SOB is a technology where the Si wafer is used as a substrate (optical bench) where the various optical components are inserted by micromachining a suitable lodging. In [244], lasers and photodetectors are inserted into etched holes in Si and bump soldered in place. The system operates at 1.55 μm with a typical bit rate of 155 Mb/s [244]. A further advantage of using a large optical mode waveguide is the ease of interfacing to a single-mode optical fiber. In the approach of [244], these are located in V-grooves etched into Si.

A fully integrated system working at 1.55 μm has been demonstrated based on Si waveguides of very small optical mode size (cross-section $0.5 \times 0.2\,\mu m^2$), which allows extremely small turn radii (1 μm) [239]. In this way a large number of optical components can be integrated on a small surface ($\geq 10\,000$ components per cm^2). Detectors are integrated within Si by using Ge hetero-growth on Si itself. a responsivity of 250 mA/W at 1.55 μm and response times shorter than 0.8 ns have been achieved [248]. Here the laser source is external to the chip and acts as a *photon battery* similarly to usual batteries for electrons.

A realistic bidirectional optical bus architecture for clock distribution on a Cray T-90 supercomputer board based on polyamide waveguides (loss of 0.21 dB/cm at 850 nm), GaAs VCSEL, and Si MSM photodetectors has been developed [255]. By using 45° total-internal-reflection mirror coupling, efficiencies as high as 100% amongst the sources or the detectors and the waveguides have been demonstrated.

7 New Directions for Silicon Lasers

As mentioned earlier, the main limitation in achieving monolithically integrated Si microphotonics is the lack of any practical Si-based light sources: either efficient LEDs or Si lasers. A laser is preferred, as incoherent emission is likely not sufficient for dense high-speed interconnects. To produce a Si laser three key ingredients are required: 1. an active material that should

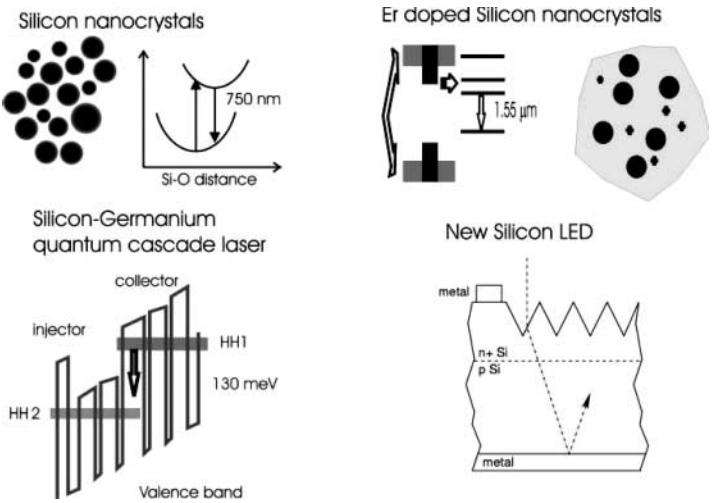

Fig. 19. Various approaches proposed to realize a silicon laser

luminesce in the region of interest and that should also be able to amplify light, 2. an optical cavity in which the active material is placed to provide the positive optical feedback, and 3. a suitable and efficient pumping scheme to achieve and sustain the laser action, preferably via electrical injection.

In the following sections, we outline some new approaches to producing Si lasers that are summarized in Fig. 19.

7.1 Bulk Silicon

Two different approaches to developing Si LEDs have been taken [256, 257]. The first approach is based on the results achieved in high efficiency solar cells and on the consideration that, within thermodynamic arguments, absorption and emission are two reciprocal processes [256]. As the first step, the non-radiative recombination rates are reduced by using high-quality intrinsic Si substrates, passivation of surfaces by high-quality thermal oxide, small metal areas, and limiting the high doping regions to contact areas. The parasitic absorption of photons, once they have been generated, is then reduced to a minimum. Finally, the extraction efficiency of light from bulk Si can be enhanced by suitably texturizing the Si surface. [256] reports the highest power efficiency to date for a Si based LED, approaching 1%. Electroluminescence spectra of these devices are typical for band-to-band recombination in Si. In addition a fully integrated opto-coupler device (LED coupled to a photodetector) was also demonstrated on the basis of this technology [258]. The main drawbacks of this approach for an integrated laser or LED are: 1. the need for both high purity (low doping concentration) and surface texturing, which renders the device processing incompatible with standard CMOS processing;

2. the strong and fast free carrier absorption typical of bulk Si, which can prevent the attainment of population inversion, is not addressed [259]; 3. appropriate integration of the active bulk Si into an optical cavity to achieve the required optical feedback to sustain laser action can be a problem; and 4. appropriate integration of the active bulk Si into an optical cavity to achieve the required optical feedback to sustain laser action can be a problem; and 5. the modulation speed of the device, which can be limited by the long lifetime of the excited carriers (milliseconds) and the need for a large optical cavity. Theoretical evidence concerning the possibility of achieving net optical gain in bulk silicon has been published recently [260].

A somewhat different approach towards achieving a reduction in the non-radiative channels in bulk Si involves exploiting the strain produced by localized dislocation loops [257, 261, 262]. Dislocations form potential pockets (i.e., energy barriers) close to the LED junction, which block the carriers and enhance radiative decay by localizing them in defect-free regions. The size of the dislocation loops was $\sim 100\,\text{nm}$, i.e., not small enough to cause quantum confinement of the carriers, and the loop distances were $\sim 20\,\text{nm}$. Free carriers injected through the top electrode are not able to diffuse away and are then constrained to recombine in the vicinity of the junction region. Onset of the EL at the band edge was observed when the diode was turned on under forward bias. No EL was observed under reverse bias. An ultimate external quantum efficiency of about 1% is claimed for these LEDs. The EL spectrum does not present significant differences in lineshape and peak position compared to that of bulk Si. A remarkable feature of this device is the high injection efficiency into the confined regions, due to the lack of quantum effects. In fact, since the density of states in the active zone is large (comparable to the bulk value), it is not a limiting factor for free carrier injection, contrary to quantum confined structures. The injection is also smooth, because there is no wide band-gap material acting as a confining barrier. This device has the additional and unexplained interesting feature of increasing efficiency with increasing temperature. The main problem of this approach for a Si laser is that it does not remove the two main problems of Auger recombination and free carrier absorption [259].

Finally, there is also a problem related to the bulk-Si LED emission wavelength, which is resonant with the Si band-gap. It is very difficult to control the region where the light is channeled in Si if these LEDs are used as a source for optical interconnects. Light will propagate throughout the wafer and will be absorbed in unwanted places.

7.2 Si/Ge Quantum Cascade Structures

One promising route that bypasses the fundamental limitation of the indirect band-gap in Si is to avoid using interband transitions. Indeed, if one exploits only intraband transitions, e.g., intravalence band transitions, no fundamental problems exist to impede lasing action in Si [263]. This is the

approach taken in the quantum cascade (QC) Si/Ge system. With Si/Ge mid-infrared QC lasers, the concept that has already proved successful for III–V semiconductors is applied [264]. The idea behind the device is shown in Fig. 19. The QC scheme can be implemented in the conduction or valence band. To achieve a conduction band discontinuity, the growth of a Si/Ge superlattice on a relaxed SiGe buffer layer is necessary. For pseudomorphic growth on a Si substrate most of the band offset occurs in the valence band. Hence, the cascading scheme is usually designed in the valence band [265]. This differs from QC lasers based on III–V semiconductors that employ electron cascade structures. In Fig. 19, the valence band diagram of a cascading stage of a hole-injected p-i-p valence band device is shown. Injected holes make a vertical transition between sub-bands, and they then cascade down the electrically biased staircase. In order to assist population inversion, the lower laser level is rapidly depopulated by relaxation within the miniband. In practice, there are two identical active regions connected by an injector. Electroluminescence from a Si/Ge QC structure grown on Si has recently been demonstrated [265,266]. The quantum efficiency estimate is about 10^{-5} for EL [266,267,268,269]. Temperature-dependent measurements show nearly identical spectra between 20 and 90 K and a broadening and vanishing of the peak at about 160 K. It is possible to improve these results by controlling the large accumulation of strain imposed by the use of a Si substrate [266].

Although the QC concept works well for III–V semiconductors, the Si/Ge system has a fundamental limit posed on the number of periods of successive cascades that is given by the critical thickness for the formation of misfit dislocations. Hence, even though these devices show interesting EL properties for the development of a Si-based laser, highly evolved cascade structures must still be realized. As the gain per single element is low, due to the nature of the intraband transition, a large number of cascading structures will be needed to accumulate a macroscopic gain. In fact, no stimulated emission in SiGe QC structures has been reported to date. In addition, these structures have to be integrated within a waveguide cavity and the emission wavelength is different from those commonly used for optical interconnects. Waveguiding at these wavelengths can be realized by using SOI substrates or thick relaxed SiGe graded buffer layers. Other needed photonic components have still to be developed to achieve a photonic integrated system. Despite this, some authors propose the use of the Si/Ge QC laser for free-air optical interconnects, but such a laser will be of little use for Si photonics if the other required elements are not developed.

7.3 Terahertz Emission

A gap in the frequency spectrum of electromagnetic waves opens up in the Terahertz (THz) region, where there were no semiconductor sources until recently. At lower frequencies, conventional sources are made via electronic oscillators (high speed transistors) while at higher frequencies the sources are

injection lasers. Recently a III–V semiconductor THz laser has been demonstrated [270]. Using the many advantages of the SiGe system over the III–V system for THz frequencies, a research effort is underway to implement the QC concept and make a laser covering this frequency region [271, 272, 273]. A typical structure employs p-type heterostructures to emit radiation from light hole–heavy hole transitions. In this way both edge emission and surface-normal THz emission might be obtained. Growth of p-Si/SiGe QC structures comprising up to 100 periods has been demonstrated using low pressure CVD via a strain-balanced approach on virtual substrates. Intersubband THz EL from a range of Si/SiGe QC structures has been observed in both edge and surface emission geometries. The light to heavy hole intersubband lifetime was measured to be ∼20 ps, which is over an order of magnitude longer than high temperature values in III–V heterostructures, implying that a Si/SiGe THz QC laser may be capable of much higher operating temperatures than corresponding III–V devices. Emission power levels comparable to those reported for III–V devices before laser processing have been measured, which indicate that there are good prospects for the realization of a THz Si/SiGe QC laser [273].

Another approach to THz laser emission in Si has also been developed [274, 275, 276, 277]. The idea is to make a THz laser using ultra-shallow donor optical transitions in Si. Very narrow spectral emission and a light intensity threshold versus pumping power were reported. These results purport that lasing has been achieved in this system. However, some points need to be clarified, such as the optical mode pattern in the simple cavity structure employed, the evolution from spontaneous to stimulated emission, and the coherent property of the light. Other concerns are related to the dilute doping of the system in order to avoid impurity–impurity interaction, which will prevent population inversion and complicate schemes for electrical injection.

7.4 Low Dimensional Silicon Structures

Light emission from quantum well and dot structures may yet hold the most promise for producing lasers at wavelengths across the visible into the infrared. The Si/SiO_2 multiple quantum well structures or silicon nanocrystals [165] are well suited for visible wavelength lasers at room temperature. We already discussed the observation of optical gain in such a system. Their optical absorption characteristics are ideal for optical pumping in a planar microcavity, but it is not yet certain if their electrical characteristics are amenable to injection laser design. Quantum dot LEDs made from $Si/Si_{1-x}Ge_x$ [203] show considerable potential for laser applications at 1.3 and possibly 1.55 μm [54]. However, much more research and development work on these structures is required before this potential can be realized.

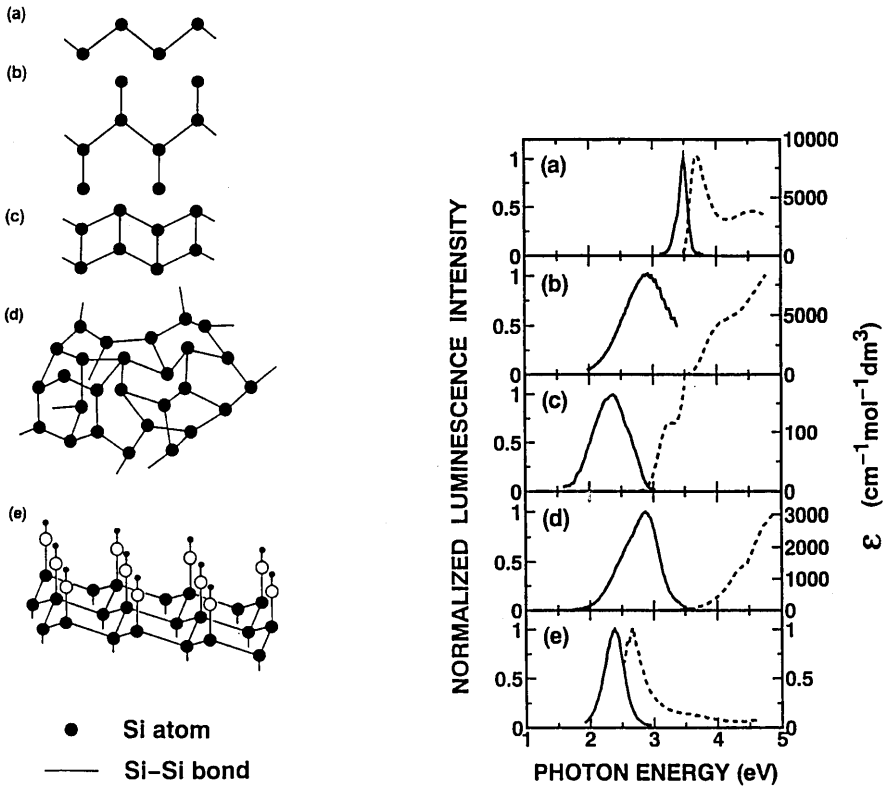

Fig. 20. Schematics of Si polymers with different backbones and their corresponding optical absorption and normalized PL spectra: (a) chain, (b) branch, (c) ladder, (d) network, and (e) planar Siloxene. After [88]

7.5 Polymers and Molecules Containing Silicon

Bright visible luminescence has been found in a number of Si polymer and molecular compounds [88,117,278]. The most prominent of these is Siloxene, $Si_6O_3H_6$, (see, for example [279]) and polysilane and its polymer derivatives (see, for example [280]).

Siloxene produces bright red PL with characteristics similar to that of the red PL in PS [281]. Its optical properties have been investigated with the hope of producing Siloxene-based devices. Siloxene has a direct band-gap [282] and the PL can be wavelength tuned across the visible region [283], but its chemical instability at higher temperatures limits its practical usefulness in devices requiring thermal processing.

Polysilane compounds are polymers based on a Si backbone with H atom termination of Si dangling bonds [284]. Derivatives of polysilane are obtained by modification of the Si skeleton structure and by the bonding of various atomic and molecular species to the backbone. Many such derivatives

are possible, including Siloxene [280, 284]. The electronic structure and optical properties of many of the simpler compounds are now understood [117]. Linear trans polysilane, $(SiH_2)_n$, comprises a zigzag one-dimensional backbone of Si atoms with each Si atom bonded to two other Si atoms and to two H atoms above and below the Si atom. As such, it can be considered the one-dimensional limit of c-Si. This form of polysilane exhibits a direct band-gap of 3.9 eV and efficiently emits ultraviolet light [88, 280]. The PL characteristics of a variety of Si polymers are shown in Fig. 20. In the case of the chain, sharp ultraviolet emission and absorption peaks are observed, which are attributed to one-dimensional excitons delocalized on the backbone chain. In the branch and ladder structures, broad PL occurs with low quantum efficiency (10^{-3}–10^{-5}) at visible wavelengths and the excitons are strongly localized. The electronic properties of two-dimensional Si backbone polymers are intermediate between those of $(SiH_2)_n$ and three-dimensional bulk Si: Either a direct or an indirect band-gap can be obtained depending on the particular configuration [280]. The PL properties of broad-band visible wavelength emission and relatively long lifetime ($\sim$ 1 ns) possessed by the branch, ladder, and network Si polymers resemble those of amorphous Si, because real polymers exhibit structural disorders. Although chain-like Si polymers possess the desired characteristics of an ultraviolet light emitter, much more development work is required before they can be considered for ultraviolet devices based on Si.

8 Conclusions

Throughout this introductory overview, we have emphasized the present status of Si microphotonics and the recent advances that have caused people to be optimistic about the realization of a practical Si light source. Indeed, there have been many claims from many of the researchers involved in this field that a Si based laser will be realized within a short period of time [285]. If this objective can be realized, all the major building blocks for monolithic Si microphotonics will then be available. The final vision is to have Si microphotonics participating in every global application of the photonics industry including communications, computing, information displays, optical and infrared imaging, medicine, optical printing, optical command and control, optical sensing of physical chemical and biological inputs, optical signal processing, optical storage, and optical control of microwave devices or systems [286]. Indeed, we propose Si as the unifying material wherein the next generation of photonic devices will be realized.

References

1. E. Kasper, F. Schäffler: Group IV Compounds. In: T. P. Pearsall: *Strained-Layer Superlattices: Materials Science and Technology.* Semiconductors and Semimetals **33** (Academic Press, Boston 1991), p. 223

2. G. Abstreiter: Phys. World **5** (3), 36 (1992)
3. P. Bhattacharya: *Semiconductor Optoelectronic Devices*, Second Edition (Prentice Hall, New York 1996)
4. B. A. Saleh, M. C. Teich: *Fundamentals of Photonics* (Wiley, New York 1991)
5. R. Soref: MRS Bull. **23** (4), 20 (1998)
6. A. Mills: III–Vs Review **15** (4), 30 (2002)
7. B. D. Dingle, M. B. Spitzer, R. W. McClelland, J. C. C. Fan, P. M. Zavracky: Appl. Phys. Lett. **62**, 2760 (1993)
8. `http://www.bookham.com`
9. R. A. Soref: Proc. IEEE **81**, 1687 (1993)
10. S. S. Iyer, Y.-H. Xie: Science **260**, 40 (1993)
11. E. A. Fitzgerald, L. C. Kimmerling: MRS Bull. **23** (4), 39 (1998)
12. K. J. Linthicum, T. Gehrke, R. F. Davis, D. B. Thomson, K. M. Tracy: U. S. Patent 6,255,198 (2001)
13. R. Droopad, Z. Yu, W. J. Ooms, J. Ramdani: U. S. Patent Application 20010013313 (2001)
14. Y. H. Lo, R. Bhat, D. M. Hwang, C. Chua, C. H. Lin: Appl. Phys. Lett. **62**, 1038 (1993)
15. K. Mori, K. Tokutome, S. Sugou: Electron. Lett. **31**, 284 (1995)
16. A. Soeno, D. Kajita, J. Suda, H. Matsunami: Jpn. J. Appl. Phys. **39**, L905 (2000)
17. J. M. London, A. H. Loomis, J. F. Ahadian, C. G. Fonstad: Photon. Tech. Lett. **11**, 958 (1999)
18. M. Sugo, H. Mori, Y. Sakai, Y. Itoh: Appl. Phys. Lett. **60**, 472 (1992)
19. R. Leon: *Silicon Monolithic Integrated Circuits in RF Systems* (Digest of Papers IEE 2001), pp. 79–87
20. A. Hoffmann, A. Rizzi (Ed.): Papers presented at the International Workshop on Nitride Semiconductors (IWN 2002), Special issue Phys. Stat. Sol. (a) **194**, (2) (2003), pp. 359–590
21. L. Pavesi, L. Dal Negro, C. Mazzoleni, G. Franzò, F. Priolo: Nature **408**, 440 (2000)
22. B. Gelloz, N. Koshida: J. Appl. Phys. **88**, 4319 (2000)
23. `http://www.eetimes.com/at/news/OEG20031104S0004`
24. `http://us.st.com/stonline/press/news/year2003/t1354h.htm`
25. `http://www.lightreading.com/document.asp?doc_id=43400`
26. T. N. Theis: IBM J. Res. Develop. **44**, 379 (2000)
27. `ftp://download.intel.com/labs/eml/download/EML_opportunity.pdf`
28. D. A. B. Miller: Proc. IEEE **88**, 728 (2000)
29. S. K. Moore: IEEE Spectrum (2002)
30. S. Ossicini, L. Pavesi, F. Priolo: *Light Emitting Silicon for Microphotonics* (Springer, Berlin, Heidelberg 2003)
31. *Properties of Silicon* (INSPEC, London 1988)
32. J. R. Chelikowsky, M. L. Cohen: Phys. Rev. B **14**, 556 (1976)
33. L. C. Kimerling, K. D. Kolenbrander, J. Michel, J. Palm: Solid State Phys. **50**, 333 (1997)
34. J. I. Pankove: *Optical Processes in Semiconductors* (Dover, New York 1971)
35. T. Trupke, J. Zhao, A. Wang, R. Corkish, M. A. Green: Appl. Phys. Lett. **82**, 2996 (2003)
36. J. R. Haynes, H. B. Briggs: Phys. Rev. **86**, 647 (1952)

37. P. J. Dean: *Luminescence of Inorganic Solids* (Academic Press, New York 1966), chap. 3
38. G. Davies: Physics Reports **176**, 83 (1989)
39. A. D. Yoffe: Advan. Phys. **42**, 173 (1993)
40. U. Gnutzman, K. Clausecker: Appl. Phys. **3**, 9 (1974)
41. S. A. Jackson, R. People: Mat. Res. Soc. Symp. Proc. **56**, 365 (1986)
42. R. People, S. A. Jackson: Phys. Rev. B **36**, 1310 (1987)
43. L. Brey, C. Tejedor: Phys. Rev. Lett. **59**, 1022 (1987)
44. S. Froyen, D. M. Wood, A. Zunger: Phys. Rev. B **36**, 4547 (1987)
45. M. S. Hybertsen, M. Schlüter: Phys. Rev. B **36**, 9683 (1987)
46. T. P. Pearsall, J. Bevk, L. C. Feldman, J. M. Bonar, J. P. Mannaerts, A. Ourmarzd: Phys. Rev. Lett. **58**, 729 (1987)
47. R. Zachai, K. Eberl, G. Abstreiter, H. Kasper, H. Kibbel: Phys. Rev. Lett. **64**, 1055 (1990)
48. U. Menczigar, G. Abstreiter, J. Olajos, H. G. Grimmeiss, H. Kibbel, H. Presting, E. Kasper: Phys. Rev. B **47**, 4099 (1993)
49. G. Abstreiter: *Light Emission in Silicon*, ed. by D. J. Lockwood (Academic Press, San Diego 1997), chap. 2
50. H. Presting, U. Menczigar, G. Abstreiter, H. Kibbel, E. Kasper: Mat. Res. Soc. Symp. Proc. **256**, 83 (1992)
51. U. Menczigar, J. Brunner, E. Freiss, M. Gail, G. Abstreiter, H. Kibbel, H. Presting, E. Kasper: Thin Solid Films **222**, 227 (1992)
52. J. Engvall, J. Olajos, H. G. Grimmeiss, H. Presting, H. Kibbel, E. Kasper: Appl. Phys. Lett. **63**, 491 (1993)
53. J. Engvall, J. Olajos, H. G. Grimmeiss, H. Kibbel, H. Presting: Phys. Rev. B **51**, 2001 (1995)
54. J. M. Baribeau, A. Delâge, S. Janz, H. Lafontaine, D. J. Lockwood, J. P. McCaffrey, S. Moisa, N. L. Rowell, D.-X. Xu: *Advanced Luminescent Materials, Quantum Confinement*, ed. by M. Cahay, S. Bandyopadhyay, N. Koshida, J. P. Leburton, D. J. Lockwood, M. Meyyappan, T. Sakamoto (Electrochemical Society, Pennington, 1999), p. 45
55. L. Vescan, T. Stoica: J. Lumin. **80**, 485 (1998)
56. H. Presting, H. Kibbel, M. Jaros, R. M. Turton, U. Menczigar, G. Abstreiter, H. G. Grimmeiss: Semicond. Sci. Technol. **7**, 1127 (1992)
57. T. P. Pearsall: Prog. Quantum Optics **18**, 97 (1994)
58. R. People, S. A. Jackson: *Strained Layer Superlattices: Physics*, ed. by T. P. Pearsall (Academic, Boston 1990), p. 119
59. D. C. Houghton, G. C. Aers, S.-R. E. Yang, E. Wang, N. L. Rowell: Phys. Rev. Lett. **75**, 866 (1995)
60. A. St. Amour, C. W. Liu, J. C. Sturm, Y. Lacroix, M. L. W. Thewalt: Appl. Phys. Lett. **67**, 3915 (1995)
61. B. A. Orner, J. Olowolafe, K. Roe, J. Kolodzey, T. Laursen, J. W. Mayer, J. Spear: Appl. Phys. Lett. **69**, 2557 (1996)
62. R. A. Soref, Z. Atzman, F. Shaapur, M. Robinson, R. Westhoff: Opt. Lett. **21**, 345 (1996)
63. J. C. Sturm: MRS Bull. **23** (4), 60 (1998)
64. N. L. Rowell, J.-P. Noël, D. C. Houghton, M. Buchanan: Appl. Phys. Lett. **58**, 957 (1990)
65. J.-P. Noël, N. L. Rowell, D. C. Houghton, D. D. Perovic: Appl. Phys. Lett. **57**, 1037 (1990)

66. J. C. Sturm, H. Manohoran, L. C. Lenchyshyn, M. L. W. Thewalt, N. L. Rowell, J.-P. Noël, D. C. Houghton: Phys. Rev. Lett. **66**, 1362 (1991)
67. L. C. Lenchyshyn, M. L. W. Thewalt, J. C. Sturm, P. V. Schwartz, E. J. Prince, N. L. Rowell, J.-P. Noël, D. C. Houghton: Appl. Phys. Lett. **60**, 3174 (1992)
68. J.-P. Noël, N. L. Rowell, D. C. Houghton, A. Wang, D. D. Perovic: Appl. Phys. Lett. **61**, 690 (1992)
69. L. C. Lenchyshyn, M. L. W. Thewalt, D. C. Houghton, J.-P. Noël, N. L. Rowell, J. C. Sturm, X. Xiao: Phys. Rev. B **47**, 16 655 (1993)
70. N. L. Rowell, J.-P. Noël, D. C. Houghton, A. Wang, L. C. Lenchyshyn, M. L.W. Thewalt, D. D. Perovic: J. Appl. Phys. **74**, 2790 (1993)
71. D. J. Robbins, P. Calcott, W. Y. Leong: Appl. Phys. Lett. **59**, 1350 (1991)
72. Q. Mi, X. Xiao, J. C. Sturm, L. C. Lenchyshyn, M. L. W. Thewalt: Appl. Phys. Lett. **60**, 3177 (1992)
73. S. Fukatsu, N. Usami, T. Chinzei, Y. Shiraki, A. Nishida, K. Nakagawa: Jpn. J. Appl. Phys. **31**, L1015 (1992)
74. Y. Kato, S. Fukatsu, Y. Shiraki: J. Vac. Sci. Technol. B **13**, 111 (1995)
75. M. Förster, U. Mantz, S. Ramminger, K. Thonke, R. Sauer, H. Kibbel, F. Schäffler, H.-J. Herzog: J. Appl. Phys. **80**, 3017 (1996)
76. H. Presting, T. Zinke, A. Splett, H. Kibbel, M. Jaros: Appl. Phys. Lett. **69**, 2376 (1996)
77. T. Stoica, L. Vescan, M. Goryll: J. Appl. Phys. **83**, 3367 (1998)
78. L. T. Canham: Appl. Phys. Lett. **57**, 1046 (1990)
79. L. Brus: Appl. Phys. A **53**, 465 (1991)
80. A. Uhlir, Jr.: Bell Syst. Tech. J. **35**, 333 (1956)
81. A. G. Cullis, L. T. Canham: Nature **353**, 335 (1991)
82. V. Lehmann, U. Gösele: Appl. Phys. Lett. **58**, 856 (1991)
83. D. C. Bensahel, L. T. Canham, S. Ossicini: *Optical Properties of Low Dimensional Structures* (Kluwer, Dordrecht 1993)
84. P. M. Fauchet, C. C. Tsai, L. T. Canham, I. Shimizu, Y. Aoyagi: *Microcrystalline Semiconductors: Materials Science and Devices* (Materials Research Society, Pittsburgh 1993)
85. D. J. Lockwood: Solid State Commun. **92**, 101 (1994)
86. Z. C. Feng, R. Tsu: *Porous Silicon* (World Scientific, Singapore 1994)
87. B. Hamilton: Semicond. Sci. Technol. **10**, 1187 (1995)
88. Y. Kanemitsu: Phys. Rep. **263**, 1 (1995)
89. J. C. Vial, J. Derrien: *Porous Silicon Science and Technology* (Springer, Berlin, Heidelberg 1995)
90. R. Hérino, W. Lang: *Porous Silicon and Related Materials* (Elsevier, Amsterdam 1995)
91. D. J. Lockwood, P. M. Fauchet, N. Koshida, S. R. J. Brueck: *Advanced Luminescent Materials* (Electrochemical Society, Pennington 1996)
92. P. M. Fauchet: J. Lumin. **70**, 294 (1996)
93. P. M. Fauchet: In: *Light Emission in Silicon*, ed. by D. J. Lockwood (Academic, San Diego 1998), chap. 6
94. A. G. Cullis, L. T. Canham, P. D. J. Calcott: J. Appl. Phys. **82**, 909 (1997)
95. P. D. J. Calcott: Mat. Sci. Eng. B **51**, 132 (1998)
96. O. Bisi, S. Ossicini, L. Pavesi: Surf. Sci. Rep. **264**, 1 (2000)
97. M. V. Wolkin, J. Jorne, P. M. Fauchet, G. Allan, C. Delarue: Phys. Rev. Lett. **82**, 197 (1999)

98. H. Mizuno, H. Koyama, N. Koshida: Appl. Phys. Lett. **69**, 3779 (1996)
99. G. Polisski, H. Heckler, D. Kovalev, M. Schwartzkoff, F. Koch: Appl. Phys. Lett. **73**, 1107 (1998)
100. F. Koch: Mater. Res. Soc. Symp. Proc. **298**, 319 (1993)
101. B. Gelloz, H. Sano, R. Boukherroub, D. D. M. Wayner, D. J. Lockwood, N. Koshida: Appl. Phys. Lett. **83**, 2342 (2003)
102. B. Gelloz, T. Nakagawa, N. Koshida: Appl. Phys. Lett. **73**, 2021 (1998)
103. K. D. Hirschman, L. Tsybeskov, S. P. Duttagupta, P. M. Fauchet: Nature **384**, 338 (1996)
104. L. Tsybeskov, S. P. Duttagupta, K. D. Hirschman, P. M. Fauchet: Appl. Phys. Lett. **68**, 2058 (1996)
105. L. Pavesi, R. Guardini, C. Mazzoleni: Solid State Commun. **97**, 1051 (1996)
106. T. Matsumoto, N. Hasegawa, T. Tamaki, K. Ueda, T. Futagi, H. Mimura, Y. Kanemitsu: Jpn. J. Appl. Phys. **33**, L35 (1994)
107. T. Matsumoto, M. Daimon, H. Mimura, Y. Kanemitsu, N. Koshida: J. Electrochem. Soc. **142**, 3528 (1995)
108. M. Ghulinyan, C. J. Oton, Z. Gaburro, P. Bettotti, L. Pavesi: Appl. Phys. Lett. **82**, 1550 (2003)
109. M. Ghulinyan, C. J. Oton, G. Bonetti, Z. Gaburro, L. Pavesi: J. Appl. Phys. **93**, 9724 (2003)
110. R. Sapienza, P. Costantino, D. Wiersma, M. Ghulinyan, C. J. Oton, L. Pavesi: Phys. Rev. Lett. **91**, 263902 (2003)
111. F. Ferrieu, A. Halimaoui, D. Bensahel: Solid State Commun. **84**, 293 (1992)
112. P. Basmaji, G. Surdutovich, R. Vitlina, J. Kolenda, V. S. Bagnato, H. Mohajerimoghaddam, N. Peyghambarian: Solid State Commun. **91**, 91 (1994)
113. I. Mihalcescu, G. Lerondel, R. Romestain: Thin Solid Films **297**, 245 (1997)
114. H. Kryzanowska, M. Kulik, J. Zuk: J. Lumin. **80**, 183 (1999)
115. D. Kovalev, G. Polisski, J. Diener, H. Heckler, N. Künzner, V. Y. Timoshenko, F. Koch: Appl. Phys. Lett. **78**, 916 (2001)
116. C. J. Oton, Z. Gaburro, M. Ghulinyan, L. Pancheri, P. Bettotti, L. Dal Negro, L. Pavesi: Appl. Phys. Lett. **81**, 4919 (2002)
117. H. Kamimura: *Light Emission from Novel Silicon Materials*, Supplement B to J. Phys. Soc. Japan **63** (Phys. Soc. Jpn., Tokyo 1994)
118. T. Ogawa, Y. Kanemitsu: *Optical Properties of Low-Dimensional Materials* (World Scientific, Singapore 1995)
119. Y. Kanemitsu: In: *Light Emission in Silicon*, ed. by D. J. Lockwood (Academic, San Diego 1998), chap. 5
120. O. Bisi, S. U. Campisano, L. Pavesi, F. Priolo: *Silicon Based Microphotonics: from Basics to Applications* (IOS Press, Amsterdam 1999)
121. L. C. Lenchyshyn, M. L. W. Thewalt, J. C. Sturm, P. V. Schwartz, E. J. Prince, N. L. Rowell, J.-P. Noël, D. C. Houghton: Appl. Phys. Lett. **60**, 3174 (1992)
122. J.-P. Noël, N. L. Rowell, D. C. Houghton, A. Wang, D. D. Perovic: Appl. Phys. Lett. **61**, 690 (1992)
123. L. C. Lenchyshyn, M. L. W. Thewalt, D. C. Houghton, J.-P. Noël, N. L. Rowell, J. C. Sturm, X. Xiao: Phys. Rev. B **47**, 16655 (1993)
124. J. Linnros: *Silicon Based Microphotonics: from Basics to Applications*, ed. by O. Bisi, S. U. Campisano, L. Pavesi, F. Priolo (IOS Press, Amsterdam 1999), pp. 47–86
125. H. Takagi, H. Ogawa, Y. Yamazaki, A. Ishizaki, T. Nakagiri: Appl. Phys. Lett. **56**, 2379 (1990)

126. S. Schuppler, S. L. Friedman, M. A. Marcus, D. L. Adler, Y.-H. Xie, F. M. Ross, T. D. Harris, W. L. Brown, Y. J. Chabal, L. E. Brus, P. H. Citrin: Phys. Rev. Lett. **72**, 2648 (1994)
127. Y. Kanzawa, T. Kageyama, S. Takeoka, M. Fujii, S. Hayashi, K. Yamamoto: Solid State Commun. **102**, 533 (1997)
128. Y. Kanemitsu, T. Ogawa, K. Shiraishi, K. Takeda: Phys. Rev. B **48**, 4883 (1993)
129. J. Valenta, R. Juhasz, J. Linnros: Appl. Phys. Lett. **80**, 1070 (2002)
130. G. Allan, C. Delerue, M. Lannoo: Phys. Rev. Lett. **76**, 2961 (1996)
131. C. Delerue, G. Allan, M. Lannoo: *Light Emission in Silicon*, ed. by D. J. Lockwood (Academic, San Diego 1998), chap. 7
132. M. Luppi, S. Ossicini: J. Appl. Phys. **94**, 2130 (2003)
133. L. E. Brus, P. F. Szajowski, W. L. Wilson, T. D. Harris, S. Schuppler, P. H. Citrin: J. Amer. Chem. Soc. **117**, 2915 (1995)
134. D. Kovalev, H. Heckler, M. Ben-Chorin, G. Polisski, M. Schwartzkopff, F. Koch: Phys. Rev. Lett. **81**, 2803 (1998)
135. T. van Buuren, L. N. Dinh, L. L. Chase, W. J. Siekhaus, L. J. Terminello: Phys. Rev. Lett. **80**, 3803 (1998)
136. N. Daldosso, M. Luppi, S. Ossicini, E. Degoli, R. Magri, G. Dalba, P. Fornasini, R. Grisenti, F. Rocca, L. Pavesi, S. Boninelli, F. Priolo, C. Bongiorno, F. Iacona: Phys. Rev. B **68**, 085327 (2003)
137. S. Tong, X.-N. Liu, L.-C. Wang, F. Yan, X.-M. Bao: Appl. Phys. Lett. **69**, 596 (1996)
138. T. Toyama, T. Matsui, Y. Kurokawa, H. Okamoto, Y. Hamakawa: Appl. Phys. Lett. **69**, 1261 (1996)
139. L. Tsybeskov, K. L. Moore, D. G. Hall, P. M. Fauchet: Phys. Rev. B **54**, R8361 (1996)
140. G. Franzo, A. Irreira, E. C. Moreira, M. Miritello, F. Iacona, D. Sanfilippo, G. F. Di Stefano, F. Fallica, F. Priolo: Appl. Phys. A **74**, 1 (2002)
141. R. T. Neal, M. D. C. Charlton, G. J. Parker, C. E. Finlayson, M. C. Netti, J. J. Baumberg: Appl. Phys. Lett. **83**, 4598 (2003)
142. L. Pavesi, L. Dal Negro, C. Mazzoleni, G. Franzò, F. Priolo: Nature **408**, 440 (2000)
143. L. Dal Negro, M. Cazzanelli, N. Daldosso, Z. Gaburro, L. Pavesi, F. Priolo, D. Pacifici, G. Franzò, F. Iacona: Physica E **16**, 297 (2003)
144. L. Khriachtchev, M. Rasanen, S. Novikov, J. Sinkkonen: Appl. Phys. Lett. **79**, 1249 (2001)
145. M. H. Nayfeh, S. Rao, N. Barry: Appl. Phys. Lett. **80**, 121 (2002)
146. K. Luterova, I. Pelant, I. Mikulskas, R. Tomasiunaset, D. Muller, J.-J. Grob, J.-L. Rehspringer, B. Honerlage: J. Appl. Phys. **91**, 2896 (2002)
147. P. M. Fauchet, J. Ruan: *Towards the First Silicon Laser*, ed. by L. Pavesi, S. Gaponenko, L. Dal Negro (Kluwer/Academic, New York 2003), p. 197
148. M. Ivanda, U. V. Densica, C. W. White, W. Kiefer: *Towards the First Silicon Laser*, ed. by L. Pavesi, S. Gaponenko, L. Dal Negro (Kluwer/Academic, New York 2003), p. 191
149. L. Dal Negro, M. Cazzanelli, Z. Gaburro, P. Bettotti, L. Pavesi, F. Priolo, G. Franzò, D. Pacifici, F. Iacona: *Towards the First Silicon Laser*, ed. by L. Pavesi, S. Gaponenko, L. Dal Negro (Kluwer/Academic, New York 2003), p. 145

150. M. Cazzanelli, Z. Gaburro, L. Dal Negro, L. Pavesi, D. Kovalev et al.: in press
151. J. Valenta, I. Pelant, J. Linnros: Appl. Phys. Lett. **81**, 1396 (2002)
152. R. G. Elliman, M. J. Lederer, N. Smith, B. Luther-Davies: Nucl. Instr. Meth. B **206**, 427 (2003)
153. L. Dal Negro, P. Bettotti, M. Cazzanelli, L. Pavesi, D. Pacifici: Optics Comm. **229**, 337 (2003)
154. L. Dal Negro, M. Cazzanelli, L. Pavesi, S. Ossicini, D. Pacifici, G. Franzò, F. Priolo, F. Iacona: Appl. Phys. Lett. **82**, 4636 (2003)
155. J. Ruan, H. Chen, P. M. Fauchet: Mat. Res. Soc. Symp. Proc. **737**, 407 (2003)
156. F. Iacona, G. Franzò, E. C. Moreira, F. Priolo: J. Appl. Phys. **89**, 8354 (2001)
157. Z. Gaburro, L. Pavesi: *Handbook of luminescence, Display Materials, and Nanocomposites*, ed. by H. S. Nalwa, L. S. Rohwer (American Scientific, Stevenson Ranch 2003)
158. G. Franzò, A. Irreira, E. C. Moreira, M. Miritello, F. Iacona, D. Sanfilippo, G. F. Di Stefano, F. Fallica, F. Priolo: Appl. Phys. A **74**, 1 (2002)
159. C. F. Lin, P. F. Chung, M. J. Chen, W. F. Su: Opt. Lett. **27**, 713 (2002)
160. L. Heikkila, T. T. Kuusela, H. P. Hedman: Superlattice. Microst. **26**, 157 (1999)
161. D. J. Lockwood, G. C. Aers, L. B. Allard, B. Bryskiewicz, S. Charbonneau, D. C. Houghton, J. P. McCaffrey, A. Wang: Can. J. Phys. **70**, 1184 (1992)
162. A. Zunger, L.-W. Wang: Appl. Surf. Sci. **102**, 350 (1996)
163. R. Tsu: Nature **364**, 19 (1993)
164. C. J. Frosch, L. Derick: J. Electrochem. Soc. **104**, 547 (1957)
165. D. J. Lockwood: Phase Transit. **68**, 151 (1999)
166. Z. H. Lu, D. J. Lockwood, J.-M. Baribeau: Nature **378**, 258 (1995)
167. D. J. Lockwood, Z. H. Lu, J.-M. Baribeau: Phys. Rev. Lett. **76**, 539 (1996)
168. D. J. Lockwood, J.-M. Baribeau, Z. H. Lu: *Advanced Luminescent Materials*, ed. by D. J. Lockwood, P. M. Fauchet, N. Koshida, S. R. J. Brueck (Electrochemical Society, Pennington 1996), p. 339
169. J. A. Brum, G. Bastard: J. Phys. C. Solid State Phys. **18**, L789 (1985)
170. Z. H. Lu, J.-M. Baribeau, D. J. Lockwood, M. Buchanan, N. Tit, C. Dharmawardana, G. C. Aers: SPIE Proc. **3491**, 457 (1998)
171. B. T. Sullivan, D. J. Lockwood, H. J. Labbé, Z.-H. Lu: Appl. Phys. Lett. **69**, 3149 (1996)
172. D. J. Lockwood, B. T. Sullivan, H. J. Labbé: J. Lumin. **80**, 75 (1999)
173. G. Pucker, P. Bellutti, C. Spinella, K. Gatterer, M. Cazzanelli, L. Pavesi: J. Appl. Phys. **88**, 6044 (2000)
174. D. J. Lockwood, M. W. C. Dharmawardana, Z. H. Lu, D. H. Grozea, P. Carrier, L. J. Lewis: Mat. Res. Soc. Symp. Proc. **737**, F1.1.1 (2003)
175. J.-B. Xia, K. W. Cheah: Phys. Rev. B **56**, 14925 (1997)
176. N. Tit, M. W. C. Dharmawardana: Solid State Commun. **106**, 121 (1998)
177. R. Tsu, Q. Zhang, A. Filios: SPIE Proc. **3290**, 246 (1997)
178. A. G. Nassiopoulou, V. Ioannou-Sougleridis, P. Photopoulos, A. Travlos, V. Tsakiri, D. Papadimitriou: Phys. Stat. Sol. (a) **165**, 79 (1998)
179. G. G. Qin, S. Y. Ma, Z. C. Ma, W. H. Zong, L. P. You: Solid State Commun. **106**, 329 (1998)
180. L. Heikkilä, T. Kuusela, H.-P. Hedman, H. Ihantola: Appl. Surf. Sci. **133**, 84 (1998)
181. Z. Gaburro, G. Pucker, P. Bellutti, L. Pavesi: Solid State Commun. **114**, 33 (2000)

182. G. Pucker, P. Bellutti, L. Pavesi: Spectrochim. Acta A **57**, 2019 (2001)
183. Y. S. Tang, C. D. W. Wilkinson, C. M. Sotomayor Torres, D. W. Smith, T. E. Whall, E. H. C. Parker: Solid State Commun. **85**, 199 (1993)
184. J. Lee, S. H. Li, J. Singh, P. K. Bhattacharaya: J. Electron. Mat. **23**, 831 (1994)
185. N. Usami, T. Mine, S. Fukatsu, Y. Shiraki: Appl. Phys. Lett. **63**, 2789 (1993)
186. N. Usami, T. Mine, S. Fukatsu, Y. Shiraki: Appl. Phys. Lett. **64**, 1126 (1994)
187. H. I. Liu, N. I. Maluf, R. F. W. Pease, D. K. Biegelsen, N. M. Johnson, F. A. Ponce: J. Vac. Sci. Technol. B **10**, 2846 (1992)
188. A. G. Nassiopoulos, S. Grigoropoulos, D. Papadimitriou: *Advanced Luminescent Materials*, ed. by D. J. Lockwood, P. M. Fauchet, N. Koshida, S. R.J. Brueck (Electrochemical Society, Pennington 1996), p. 296
189. S. H. Zaidi, A.-S. Chu, S. R. J. Brueck: In: *Advanced Luminescent Materials*, ed. by D. J. Lockwood, P. M. Fauchet, N. Koshida, S. R. J. Brueck (Electrochemical Society, Pennington 1996), p. 307
190. A. G. Nassiopoulos, S. Grigoropoulos, D. Papadimitriou: Appl. Phys. Lett. **69**, 2267 (1996)
191. H. Namatsu, K. Kurihara, M. Nagase, T. Makino: Appl. Phys. Lett. **70**, 619 (1997)
192. H. I. Liu, D. K. Biegelsen, F. A. Ponce, N. M. Johnson, R. F. W. Pease: Appl. Phys. Lett. **64**, 1363 (1994)
193. V. V. Poborchii, T. Tada, T. Kanayama: J. Appl. Phys. **91**, 3299 (2002)
194. Y. F. Zhang, Y. H. Tang, N. Wang, D. P. Yu, C. S. Lee, I. Bello, S. T. Lee: Appl. Phys. Lett. **72**, 1835 (1998)
195. D. P. Yu, Z. G. Bai, J. J. Wang, Y. H. Zou, W. Qian, J. S. Fu, H. Z. Zhang, Y. Ding, G. C. Xiong, L. P. You, J. Xu, S. Q. Feng: Phys. Rev. B **59**, R2498 (1999)
196. X.-H. Sun, Y.-H. Tang, P. Zhang, S. J. Naftel, R. Sammynaiken, T. K. Sham, H. Y. Peng, Y.-F. Zhang, N. B. Wong, S. T. Lee: J. Appl. Phys. **89**, 6396 (2001)
197. F. C. K. Au, K. W. Wong, Y. H. Tang, Y. F. Zang, I. Bello, S. T. Lee: Appl. Phys. Lett. **75**, 1700 (1999)
198. Y. H. Tang, X. H. Sun, F. C. K. Au, L. S. Liao, H. Y. Peng, C. S. Lee, S. T. Lee, T. K. Sham: Appl. Phys. Lett. **79**, 1673 (2001)
199. F. Buda, J. Kohanoff: Prog. Quant. Electr. **18**, 201 (1994)
200. S. Ossicini, C. M. Bertoni, M. Biagini, A. Lugli, G. Roma, O. Bisi: Thin Solid Films **297**, 154 (1997)
201. Y. S. Tang, C. M. Sotomayor Torres, R. A. Kubiak, D. A. Smith, T. E. Whall, E. H. C. Parker, H. Presting, H. Kibbel: *The Physics of Semiconductors*, vol. 2, ed. by D. J. Lockwood (World Scientific, Singapore 1995), p. 1735
202. R. Apetz, L. Vescan, A. Hartmann, C. Dieker, H. Lüth: Appl. Phys. Lett. **66**, 445 (1995)
203. Y. S. Tang, W.-X. Ni, C. M. Sotomayor Torres, G. V. Hansson: Electron. Lett. **31**, 1385 (1995)
204. L. Tsybeskov, K. D. Hirschman, S. P. Duttagupta, M. Zacharias, P. M. Fauchet, J. P. McCaffrey, D. J. Lockwood: Appl. Phys. Lett. **72**, 43 (1998)
205. J. Ruan, P. M. Fauchet, L. Dal Negro, M. Cazzanelli, L. Pavesi: Appl. Phys. Lett. **83**, 5479 (2003)
206. D. G. Thomas, M. Gershenzon, J. J. Hopfield: Phys. Rev. **131**, 2397 (1963)

207. H. Ennen, G. Pomrenke, A. Axmann, K. Eisele, W. Haydl, J. Schneider: Appl. Phys. Lett. **46**, 381 (1985)
208. L. T. Canham, K. G. Barraclough, D. J. Robbins: Appl. Phys. Lett. **51**, 1509 (1987)
209. P. L. Bradfield, T. G. Brown, D. G. Hall: Appl. Phys. Lett. **55**, 100 (1989)
210. T. G. Brown, D. G. Hall: *Light Emission in Silicon*, ed. by D. J. Lockwood (Academic Press, San Diego 1998), chap. 3
211. T. G. Brown, D. G. Hall: Appl. Phys. Lett. **49**, 245 (1986)
212. G. H. Dieke: *Spectra and Energy Levels of Rare Earth Ions in Crystals* (Wiley, New York 1968)
213. H. Ennen, J. Schneider, G. Pomrenke, A. Axmann: Appl. Phys. Lett. **43**, 943 (1983)
214. J. Michel, L. V. C. Assali, M. T. Morse, L. C. Kimmerling: *Light Emission in Silicon*, ed. by D. J. Lockwood (Academic, San Diego 1998), chap. 4
215. S. Coffa, G. Franzò, F. Priolo: MRS Bulletin **23** (4), 25 (1998)
216. J. Michel, B. Zheng, J. Palm, E. Ouellette, F. Gan, L. C. Kimerling: Mat. Res. Soc. Symp. Proc. **422**, 317 (1996)
217. J. Stimmer, A. Reittinger, G. Abstreiter, H. Holzbrecher, Ch. Buchal: Mat. Res. Soc. Symp. Proc. **422**, 15 (1996)
218. S. Coffa, G. Franzò, F. Priolo: Appl. Phys. Lett. **69**, 2077 (1996)
219. L. Tsybeskov, S. P. Duttagupta, K. D. Hirschman, P. M. Fauchet, K. L. Moore, D. G. Hall: Appl. Phys. Lett. **70**, 1790 (1997)
220. G. Franzò, S. Coffa, F. Priolo, C. Spinella: J. Appl. Phys. **81**, 2784 (1997)
221. G. Franzò, V. Vinciguerra, F. Priolo: Appl. Phys. a **69**, 3 (1999)
222. G. Franzò, D. Pacifici, V. Vinciguerra, F. Priolo, F. Iacona: Appl. Phys. Lett. **76**, 2167 (2000)
223. M. Zacharias, M. S. J. Heitmann, P. Streitenberger: Physica E **11**, 245 (2001)
224. P. G. Kik, A. Polman: *Towards the First Silicon Laser*, ed. by L. Pavesi, S. Gaponenko, L. Dal Negro (Kluwer/Academic, New York 2003), p. 383
225. F. Iacona, D. Pacifici, A. Irrera, M. Miritello, G. Franzó, F. Priolo, D. Sanfilippo, G. Di Stefano, P. G. Fallica: Appl. Phys. Lett. **81**, 3242 (2002)
226. M. E. Castagna, S. Coffa, L. Caristia, A. Messina, C. Bongiorno: Proceedings of ESSDDERC 2002 (2002), p. 439
227. X. Zhao, S. Komuro, H. Isshiki, Y. Aoyagi, T. Sugano: Appl. Phys. Lett. **74**, 120 (1999)
228. H.-S. Han, S.-Y. Seo, J. H. Shin: Appl. Phys. Lett. **79**, 4568 (2001)
229. H.-S. Han, S.-Y. Seo, J. H. Shin, N. Park: Appl. Phys. Lett. **81**, 3720 (2002)
230. F. Priolo, G. Franzò, D. Pacifici, V. Vinciguerra, F. Iacona, A. Irrera: J. Appl. Phys. **89**, 264 (2001)
231. A. J. Kenyon, C. E. Chryssou, C. W. Pitt, T. Shimizu-Iwayama, D. E. Hole, N. Sharma, C. J. Humphreys: J. Appl. Phys. **91**, 367 (2002)
232. P. G. Kik, A. Polman: J. Appl. Phys. **91**, 534 (2002)
233. G. Masini, L. Colace, G. Assanto: Mat. Sci. Eng. B **89**, 2 (2002)
234. B. P. Pal: *Progress in Optics XXXII*, ed. by E. Wolf (Elsevier, Amsterdam 1993), p. 1
235. T. Miya: IEEE J. Sel. Top. Quantum Electron. **6**, 38 (2000)
236. D. A. P. Bulla, B. V. Borges, M. A. Romero, N. I. Morimoto, L. G. Neto, A. L. Cortes: IMOC'99 IEEE Proc. (1999), p. 454
237. U. Hilleringmann, K. Goser: IEEE Trans. Electron. Dev. **42**, 841 (1995)

238. G. Cocorullo, F. G. Della Corte, M. Iodice, I. Rendina, P. M. Sarro: IEEE J. Sel. Top. Quantum Electron. **4**, 983 (1998)
239. L. C. Kimerling: Appl. Surf. Science **159–160**, 8 (2000)
240. K. K. Lee, D. R. Lim, H.-C. Luan, A. Agarwal, J. Foresi, L. C. Kimerling: Appl. Phys. Lett. **77**, 1617 (2000)
241. M. A. Rosa, N. Q. Ngo, D. Sweatman, S. Dimitrijev, H. B. Harrison: IEEE J. Sel. Top. Quantum Electron. **5**, 1249 (1999)
242. T. W. Ang, G. T. Reed, A. Vonsovici, A. G. R. Evans, P. R. Routley, M. R. Josey: Electron. Lett. **35**, 977 (1999)
243. B. Jalali, S. Yegnanarayanan, T. Yoon, T. Yoshimoto, I. Rendina, F. Coppinger: IEEE J. Sel. Top. Quantum Electron. **4**, 938 (1998)
244. T. Bestwick: Proc. 48th IEEE Electronic Components and Technology Conference, 25–28 May 1998 (1988), pp. 566–571
245. H. Zimmermann: *Integrated Silicon Optoelectronics* (Springer, New York 2000)
246. S. M. Csutak, J. D. Schaub, W. E. Wu, R. Shimer, J. C. Campbell: J. Lightwave Technol. **20**, 1724 (2002)
247. M. Yang, K. Rim, D. L. Rogers, J. D. Schaub, J. J. Wleser, D. M. Kuchta, D. C. Boyd, F. Rodier, P. A. Rabidoux, J. T. Marsh, A. D. Icknor, Q. Yang, A. Upham, S. C. Ramac: IEEE Elect. Dev. Lett. **23**, 395 (2002)
248. G. Masini, L. Colace, G. Assanto, K. Wada, L. C. Kimerling: Electron. Lett. **35**, 1467 (1999)
L. Colace, G. Masini, G. Assanto, H. C. Luan, K. Wada, L. C. Kimerling: Appl. Phys. Lett. **76**, 1231 (2000)
249. S. Winnerl, D. Buca, S. Lenk, Ch. Buchal, S. Mantl, D. X. Xu: Mat. Sci. Eng. B **89**, 73 (2002)
250. M. El kurdi, P. Boucaud, S. Sauvage, G. Fishman, O. Kermarrec, Y. Campidelli, D. Bensahel, G. Saint-Girons, I. Sagnes, G. Patriarche: J. Appl. Phys. **92**, 1858 (2002)
251. D.-X. Xu, S. Janz, H. Lafontaine, M. R. T. Pearson: SPIE Proc. **3630**, 50 (1999)
252. G. Coppola, A. Irace, G. Breglio, M. Iodice, L. Zeni, A. Cutulo, P. M. Sarro: Optics Laser Eng. **39**, 317 (2003)
253. C. Fernando, S. Janz, N. G. Tarr, R. Normandin, J.-P. Noël, J. S. Wight: SPIE Proc. **2402**, 131 (1995)
254. K. Kato, Y. Tohmori: IEEE J. Sel. Top. Quantum Electron. **6**, 4 (2000)
255. R. T. Chen, L. Lin, C. Choi, Y. J. Liu, B. Bihari, L. Wu, S. Tang, R. Wickman, B. Picor, M. K. Hibbs-Brenner, J. Bristow, Y. S. Liu: IEEE Proc. **88**, 780 (2000)
256. M. A. Green, J. Zhao, A. Wang, P. J. Reece, M. Gal: Nature **412**, 805 (2001)
257. W. L. Ng, M. A. Lourenço, R. M. Gwilliam, S. Ledain, G. Shao, K. P. Homewood: Nature **410**, 192 (2001)
258. J. Zhao, M. A. Green, A. Wang: J. Appl. Phys. **92**, 2977 (2002)
259. W. P. Dumke: Phys. Rev. **127**, 1559 (1962)
260. T. Trupke, M. Green: J. Appl. Phys. **93**, 9058 (2003)
261. C. Delerue, M. Lannoo, G. Allan, E. Martin, I. Mihalcescu, J. C. Vial, R. Romestain, F. Muller, A. Bsiesy: Phys. Rev. Lett. **75**, 2229 (1995)
262. P. Jonsson, H. Bleichner, M. Isberg, E. Nordlander: J. Appl. Phys. **81**, 2256 (1997)

263. R. A. Soref: Thin Solid Films **294**, 325 (1997)
264. C. Gmachl, F. Capasso, D. L. Sivco, A. Y. Cho: Rep. Prog. Phys. **64**, 1533 (2001)
265. G. Dehlinger, L. Diehl, U. Gennser, H. Sigg, J. Faist, K. Ensslin, D. Grützmacher: Science **290**, 2277 (2000)
266. L. Diehl, S. Mentese, H. Sigg, E. Müller, D. Grützmacher, U. Gennser, I. Sagnes, T. Fromherz, J. Stangl, T. Roch, G. Bauer, Y. Campidelli, O. Kermarrec, D. Bensahel, J. Faist: Appl. Phys. Lett. **81**, 4700 (2002)
267. G. Dehlinger, L. Diehl, U. Gennser, H. Sigg, E. Muller, S. Stutz, J. Faist, J. Stangl, T. Roch, G. Bauer, D. Grützmacher: Mat. Sci. Eng. B **89**, 30 (2002)
268. L. Diehl, S. Mentese, H. Sigg, E. Müller, D.Grützmacher, U. Gennser, I. Sagnes, T. Fromherz, J. Stangl, T. Roch, G. Bauer, Y. Campidelli, O. Kermarrec, D. Bensahel, J. Faist: *Towards the First Silicon Laser*, ed. by L. Pavesi, S. Gaponenko, L. Dal Negro (Kluwer/Academic, New York 2003), p. 325
269. I. Bormann, K. Brunner, S. Hackenbuchner, G. Zandler, G. Abstreiter, S. Schmult, W. Wegscheider: Appl. Phys. Lett. **80**, 2260 (2002)
270. R. Kohler, A. Tredicucci, F. Beltram, H. Beere, E. Linfield, G. Davies, D. Ritchie, R. C. Iotti, F. Rossi: Nature **417**, 156 (2002)
271. S. A. Lynch, R. Bates, D. J. Paul, D. J. Norris, A. G. Cullis, Z. Ikonic, R. W. Kelsall, P. Harrison, D. D. Arnone, C. R. Pidgeon: Appl. Phys. Lett. **81**, 1543 (2002)
272. S. A. Lynch, S. S. Dhillon, R. Bates, D. J. Paul, D. D. Arnone, D. J. Robbins, Z. Ikonic, R. W. Kelsall, P. Harrison, D. J. Norris, A. G. Cullis, C. R. Pidgeon, P. Murzyn, A. Loudon: Mat. Sci. Eng. B **89**, 10 (2002)
273. R. W. Kelsall, Z. Ikonic, P. Harrison, S. A. Lynch, R. Bates, D. J. Paul, D. J. Norris, S. L. Liew, A. G. Cullis, D. J. Robbins, P. Murzyn, C. R. Pidgeon, D. D. Arnone, R. A. Soref: *Towards the First Silicon Laser*, ed. by L. Pavesi, S. Gaponenko, L. Dal Negro (Kluwer/Academic, New York, 2003), p. 367
274. S. G. Pavlov, H.-W. Hübers, M. H. Rümmeli, J. N. Hovenier, T. O. Klaasen, R. Kh. Zhukavon, A. V. Muravjov, V. N. Shastin: *Towards the First Silicon Laser*, ed. by L. Pavesi, S. Gaponenko, L. Dal Negro (Kluwer/Academic, New York, 2003), p. 331
V. N. Shastin, E. E. Orlova, R.Kh.Zhukavin, S. G. Pavlov, H.-W. Hübers, H. Riemann: *Towards the First Silicon Laser*, ed. by L. Pavesi, S. Gaponenko, L. Dal Negro (Kluwer/Academic, New York 2003), p. 341
275. N. Shastin, R. Kh. Zhukavin, E. E. Orlova, S. G. Pavlov, M. H. Rummeli, H.-W. Hubers, J. N. Hovenier, T. O. Klaassen, H. Riemann, I. V. Bradley, A. F. G. van der Meer: Appl. Phys. Lett. **80**, 3512 (2002)
276. A. Blom, M. A. Odnoblyudov, H. H. Cheng, I. N. Yassievich, K. A. Chao: Appl. Phys. Lett. **79**, 713 (2001)
277. S. G. Pavlov, R. Kh. Zhukavin, E. E. Orlova, V. N. Shastin, A. V. Kirsanov, H.-W. Hubers, K. Auen, H. Riemann: Phys. Rev. Lett. **84**, 5220 (2000); S. G. Pavlov, H.-W. Hubers, H. Riemann, R. Kh. Zhukavin, E. E. Orlova, V. N. Shastin: J. Appl. Phys. **92**, 5632 (2002)
278. L. E. Brus: *Light Emission in Silicon*, ed. by D. J. Lockwood (Academic Press, San Diego 1998), chap. 8
279. M. Stutzmann, M. S. Brandt, H. D. Fuchs, M. Rosenbauer, M. K. Kelly, P. Deak, J. Weber, S. Finkbeiner: *Optical Phenomena in Semiconductor Struc-*

tures of Reduced Dimensions, ed. by D. J. Lockwood, A. Pinczuk (Kluwer, Dordrecht 1993), p. 427
280. K. Takeda: *Light Emission from Novel Silicon Materials*, ed. by H. Kamimura (Physical Society of Japan, Tokyo 1994), p. 1
281. M. S. Brandt, H. D. Fuchs, M. Stutzmann, J. Weber, M. Cardona: Solid State Commun. **81**, 307 (1992)
282. P. Deák, M. Rosenbauer, M. Stutzmann, J. Weber, M. S. Brandt: Phys. Rev. Lett. **69**, 2531 (1992)
283. M. Stutzmann, M. S. Brandt, M. Rosenbauer, H. D. Fuchs, S. Finkbeiner, J. Weber, P. Deak: J. Lumin. **57**, 321 (1993)
284. R. D. Miller, J. Michl: Chem. Rev. **89**, 1359 (1989)
285. N. Ascombe: Seeking a Silicon Laser, Photonics Spectra (February 2003), p. 62
286. R. A. Soref: *Silicon Based Microphotonics: from Basics to Applications*, ed. by O. Bisi, S. U. Campisano, L. Pavesi, F. Priolo (IOS Press, Amsterdam 1999), p. 1

Index